Asian Journal of Chemistry; Vol. 38, No. 4 (2026), 921-937
ASIAN JOURNAL OF CHEMISTRY
https://doi.org/10.14233/ajchem.2026.35235

Synthesis, Characterisation, DFT and Docking Analysis of 3-Methyl-2,6-*bis*(3-methylphenyl)piperidin-4-one (MBMP) as Anti-Retroviral Therapeutic Agent

J. GERSHOM STUART and J. WINFRED JEBARAJ*

Department of Chemistry, St. John's College (Affiliated to Manonmaniam Sundaranar University, Abishekapatti), Palayamkottai, Tirunelveli-627002, India

*Corresponding author: E-mail: winfred.chem@stjohnscollege.edu.in

Received: 11 November 2025 *Accepted*: 20 January 2026 *Published online*: 8 April 2026 AJC-22313

RNA is vital in HIV gene expression and replication. Despite antiretroviral therapy (ART) advancements, the high mutation of HIV rate remains challenging. In this work, the synthesis, quantum chemical analysis and molecular docking of 3-methyl-2,6-*bis*(3-methylphenyl)piperidin-4-one (MBMP) were carried out to evaluate its potential as an anti-retroviral therapeutic agent. The synthesized MBMP was structurally confirmed through standard spectroscopic techniques and its molecular geometry along with electronic properties were further optimized using density functional theory (DFT) calculations performed with Gaussian 16W in the gas phase. The electronic structure of the optimised structure has been identified through the density functional theory (DFT) approach. All calculations were performed at the B3LYP/6-311G(d,p) level of theory and the resulting HOMO–LUMO energies were analyzed to elucidate the system's stability, reactivity and electronic properties. The Fukui function was determined to identify reactive sites within the molecule, while Mulliken population analysis was employed to evaluate the charge distribution on individual atoms. Molecular electrostatic potential (MEP) analysis was employed to identify electron-rich and electron-deficient regions, while natural bond orbital (NBO) analysis provided insight into molecular stability. Further analyses, including non-covalent interactions (NCI), scanning tunneling microscopy (STM), aromaticity and LOL-based shaded surface maps, were carried out using Multiwfn 3.8, while UV and NMR spectroscopy validated structural integrity and purity, and binding interactions were elucidated using Discovery Studio Visualizer.

Keywords: Piperidinone, Fukui functions, Non-covalent interactions, Scanning tunneling microscopy, Docking studies.

INTRODUCTION

Piperidone-related compounds, such as piperine, are characterized by a conjugated system of double bonds and a piperidine ring, which contribute to their lipophilicity and ability to interact with biological membranes and enzymes [1]. The electron-rich regions of the molecule can form non-covalent interactions, including hydrogen bonding, π–π stacking and van der Waals contacts, with key sites in cytochrome P450 enzymes and efflux transporters like P-glycoprotein [2,3]. These interactions inhibit enzymatic metabolism and efflux of co-administered drugs, such as nevirapine, thereby enhancing their systemic availability. From a pharmacochemical perspective, the methylenedioxyphenyl moiety of piperine is particularly important for stabilizing enzyme-inhibitor complexes [4,5], while the flexible piperidine ring allows optimal conformational adaptation to active sites [6]. Based on facts, these structural features enable piperidone-related compounds to act as bioenhancers, improving both the pharmacokinetics and efficacy of conventional HIV treatments.

In the human immunodeficiency virus (HIV), ribonucleic acid (RNA) plays a crucial role in replication and gene regulation. Alterations in RNA significantly influence HIV-1 gene expression and replication [7]. HIV exists as two main types, HIV-1 and HIV-2, both being single-stranded positive-sense RNA viruses. HIV-1 is the predominant type associated with acquired immunodeficiency syndrome (AIDS) [8-10]. The rapid mutation rate of HIV-1 enables it to dodge the immune responses, making treatment challenging [10]. Antiviral strategies focus on inhibiting key viral enzymes, such as reverse transcriptase and protease. Highly active antiretroviral therapy (HAART) combines nucleoside reverse transcriptase inhibitors (NRTIs) with either non-nucleoside reverse transcriptase inhi-

bitors (NNRTIs) or protease inhibitors to block viral replication [11-13].

HIV protease inhibitors (PIs) are critical in therapy, with early drugs including saquinavir, nelfinavir (NFV), indinavir, ritonavir and fosamprenavir, a prodrug of amprenavir [14,15]. Subsequent PIs such as lopinavir, atazanavir, tipranavir, and darunavir were developed to improve efficacy and resistance profiles. Studies on inhibitors like KNI-1657 show enhanced binding affinity to mutant HIV-1 proteases, driven by van der Waals and electrostatic interactions, highlighting the importance of molecular interactions in drug design [16].

Density functional theory (DFT) serves as an effective approach for understanding biological activity by providing detailed insights into the electronic properties of molecules, which are essential for predicting their reactivity in various chemical environments [17,18]. Such analyses are particularly relevant for piperidone derivatives, as their electronic characteristics may contribute to improved interaction with biological targets, thereby potentially enhancing the efficacy of conventional HIV treatments through better drug metabolism and activity [19]. The present study focuses on investigating the molecular structure, electronic properties and reactive sites of the 3-methyl-2,6-bis(3-methyl-phenyl)piperidin-4-one (MBMP) compound using DFT calculations. In addition, molecular docking analysis is performed to understand its interaction with biological targets. The study also seeks to correlate theoretical findings with experimental spectral data to assess its stability, reactivity and therapeutic relevance.

COMPUTATIONAL METHOD

The Gaussian 16W package's [20] density functional theory technique is chosen to explain all of the theoretical computations. The chosen basis set is 6-311G(d,p). The preferred density function is B3LYP [21]. A molecular visualisation tool called GaussView 06 is used to observe the properties of molecules [22]. Bond angle, bond length and dihedral angle are among the structural properties that have been calculated theoretically. The aforementioned basis set and DFT methodologies have been utilised to find out the target molecule's electronic structure. Some physical properties of the molecule are also predicted using NBO analysis, Mulliken population analysis and MEP. Various reactivity parameters are computed using HOMO and LUMO values. Non-covalent interactions, the localised orbital locator (LOL), the electron localisation function (ELF) [23] and other topics are examined. The Multiwfn 3.8 platform analyzes reduced density gradients [24] and the Visual Molecular Dynamics 1.9.3 (VMD) package [25,26] visualizes them.

EXPERIMENTAL

Synthesis: Compound 3-methyl-2,6-*bis*(3-methyl-phenyl)-piperidin-4-one (MBMP) was synthesized following a modified procedure based on the method reported by Noller & Baliah [27]. Ammonium acetate (0.05 mol) was dissolved in 60 mL of absolute ethanol and mixed with 3-methylbenzaldehyde (0.1 mol) and ethyl methyl ketone (0.05 mol). The reaction mixture was refluxed in a 250 mL round-bottom flask for 30 min and then allowed to stand undisturbed at room temperature overnight to facilitate product formation. The resulting crude product was separated, washed with ethanol to remove the impurities and subsequently purified through recrystallization using ethanol (**Scheme-I**). The purified solution was filtered using Whatman No. 41 filter paper and stored. To obtain the acidic form, the free base was treated with conc. HCl in an ether medium. The resulting hydrochloride salt was further purified by recrystallization. Subsequently, the free base was regenerated by treating the hydrochloride with aqueous NH_3 solution in an alcoholic medium, followed by dilution with water to induce precipitation. The final product was obtained as well-defined crystals after allowing the solution to stand for 7-10 days, yielding a high-purity compound.

Characterisation: UV-Vis spectra of the sample were recorded using a JASCO V-530 dual beam spectrophotometer in the wavelength range of 200-900 nm after dissolving the sample in ethanol. The ^{1}H NMR spectrum was obtained on a Bruker 400 MHz spectrometer, with the sample prepared by dissolving 20 mg of compound in 0.5 mL of DMSO-d_6 containing 0.03% TMS and recorded with 16 scans. The ^{13}C NMR spectrum was also recorded on a Bruker 400 MHz instrument operating at 100 MHz using a similar sample preparation, with spectral data acquired over 1024 scans.

Docking analysis: The X-ray crystal structure of HIV-1 protease (PDB ID: 5YOK) complexed with a hydrolase inhibitor, with a resolution of 0.85 Å, was retrieved from the Protein Data Bank (https://www.rcsb.org/structure/5YOK) [28]. A library of 38,361 piperidone derivatives (57 series comprising 673 molecules each) was designed using ChemSketch software [29], incorporating various substituents such as Cl, Br, I, NH_2, OH, OMe and NO_2 at different positions on the benzene rings in mono-, di- and tri-substituted forms. All the designed compounds were subjected to energy minimization using the Avogadro tool [30] prior to molecular docking and the most

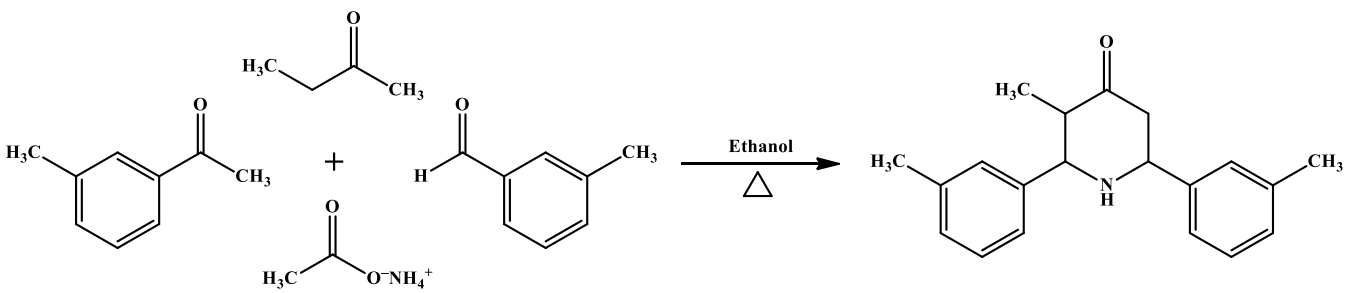

Scheme-I: Synthesis of 3-methyl-2,6-*bis*(3-methylphenyl)piperidin-4-one (MBMP)

favourable docking model was selected for further analysis. The energy minimised structures are saved as PDB format. The prepared 5YOK protein may potentially dock with the designed 673 piperidin-4-one ligands (a complete series). The PyRx software [31] and AutoDock program [32] have been used for docking. Docking results were analyzed and visualized using PyMOL [33], while molecular interactions and binding modes were further examined using Discovery Studio Visualizer.

Ligand 3-methyl-2,6-*bis*(3-methylphenyl)piperidin-4-one was identified as the most promising candidate, exhibiting a binding affinity of -7.6 kcal/mol. FDA-approved HIV-1 drugs were also docked against the target protein for comparison, and their binding affinities were evaluated. These comparative results have been reported in our previous study [34].

RESULTS AND DISCUSSION

Optimised parameters of the target molecule

Atom list: 3-Methyl-2,6-*bis*(3-methylphenyl)piperidin-4-one (MBMP) is a compound with the molecular formula $C_{20}H_{23}NO$. The 2D and 3D structures of the molecule are presented in Fig. 1, while the atom numbering scheme is shown in Table-1. The molecule consists of 45 atoms, including 20 carbon, 23 hydrogen, one nitrogen and one oxygen atom, with a total of 158 electrons. It exists in a neutral singlet state. The piperidone ring is formed by carbon atoms C1, C2, C3, C5 and C6, whereas the remaining carbon atoms are distributed in the side chains and two six-membered aromatic rings.

TABLE-1
ATOMIC INFORMATION OF THE MBMP MOLECULE

1	C	10	C	19	O	28	H	37	H
2	C	11	C	20	C	29	H	38	H
3	C	12	C	21	C	30	H	39	H
4	N	13	C	22	C	31	H	40	H
5	C	14	C	23	H	32	H	41	H
6	C	15	C	24	H	33	H	42	H
7	C	16	C	25	H	34	H	43	H
8	C	17	C	26	H	35	H	44	H
9	C	18	C	27	H	36	H	45	H

Bond length interpretation: The bond lengths of the MBMP molecule were calculated using the specified level of theory. The structure comprises twenty one C–C, twenty two C–H, two C–N, one N–H and one C=O bond. Within the piperidone ring, the C–C bond lengths show noticeable variation rather than uniformity. As presented in Table-2, bonds adjacent to substituent groups exhibit slight shortening or elongation, which can be attributed to the influence of electron-donating and electron-withdrawing groups on the ring system [35].

Since, the piperidone ring contains the electronegative replacements C3-O19 and N4-H26, the bond length for C–C in the current work is approximately 1.5 Å. In contrast, C2-N4 and C6-N4 bonds have bond lengths of 1.4748 Å and 1.4781 Å, respectively. The valence electron cloud of the H-atom is strongly attracted by the carbon atoms of the phenyl ring in the substituted piperidone, which causes the C–C bond lengths to decrease by about 1.39 Å. For alkyl groups, piperidone ring and phenyl rings, the C-H bond lengths are determined to be typical C-H single bond lengths of 1.08 Å. The carbon bond lengths of C1–C2 and C1–H23 are computed to be 1.5428 Å and 1.0949 Å, respectively. These values will be expected for the piperidone ring's electronegative nitrogen atom relationship. The longest bond length in the MBMP molecule is observed between C5 and C6 (1.5575 Å), which can be influenced by the presence of nearby substituent groups. In contrast, the shortest bond is between N4 and H26 (1.0132 Å), likely due to the strong interaction involving the electronegative nitrogen atom in the piperidone ring. The bond lengths of C2–N4 (1.4748 Å) and C6–N4 (1.4781 Å) are longer compared to the C3=O19 bond (1.2127 Å), which is shorter due to the higher electronegativity and double bond character of oxygen.

Bond angle interpretation: The bond angles of the optimized MBMP molecule were calculated using the same level of theory. The C6–N4–H26 bond angle was found to be 109.743º, which is close to the ideal tetrahedral angle of 109.5º, but shows slight deviation due to the presence of a lone pair of electrons on the nitrogen atom. The bond angles around N4 [C2–N4–C6 = 119.725º, C2–N4–H26 = 110.423º and C6–N4–

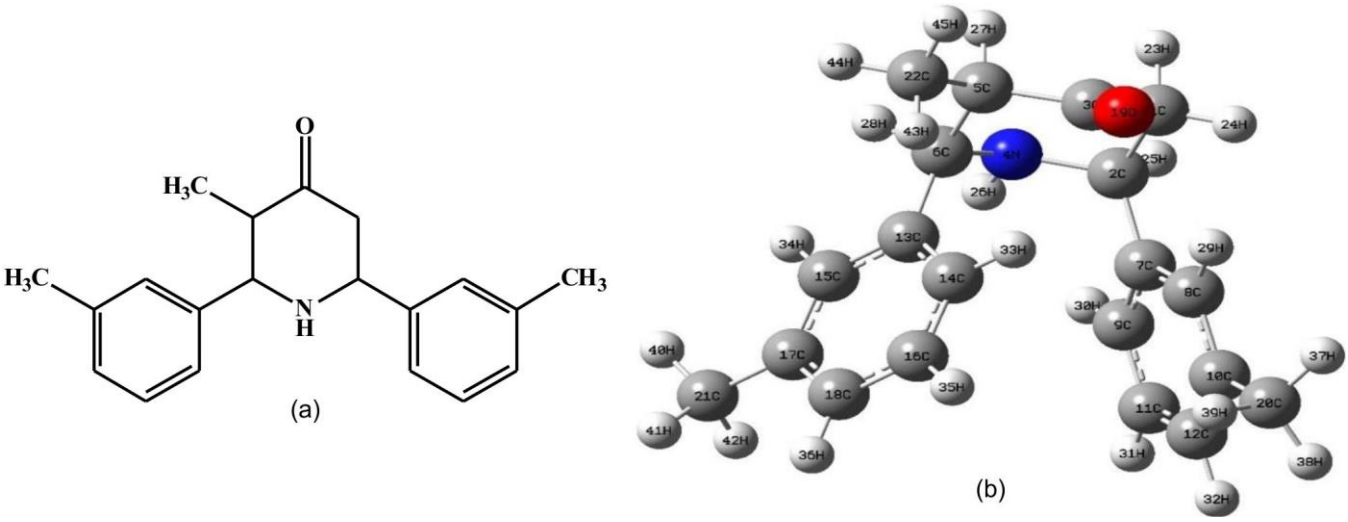

Fig. 1. (a) 2D and (b) optimised 3D structure of MBMP molecule

TABLE-2
BOND LENGTH VALUES OF MBMP MOLECULE (OPTIMIZED STRUCTURE)

S. No.	Atom set	Bond distance (Å)	S. No.	Atom set	Bond distance (Å)	S. No.	Atom set	Bond distance (Å)
1	(C1-C2)	1.5428	17	(C7-C8)	1.3958	33	(C15-H34)	1.0877
2	(C1-C3)	1.5191	18	(C7-C9)	1.4006	34	(C16-C18)	1.3909
3	(C1-H23)	1.0949	19	(C8-C10)	1.4012	35	(C16-H35)	1.0845
4	(C1-H24)	1.0893	20	(C8-H29)	1.084	36	(C17-C18)	1.3979
5	(C2-N4)	1.4748	21	(C9-C11)	1.3887	37	(C17-C21)	1.5102
6	(C2-C7)	1.5376	22	(C9-H30)	1.0861	38	(C18-H36)	1.0854
7	(C2-H25)	1.0961	23	(C10-C12)	1.3948	39	(C20-H37)	1.0927
8	(C3-C5)	1.5242	24	(C10-C20)	1.5103	40	(C20-H38)	1.0922
9	(C3-O19)	1.2127	25	(C11-C12)	1.3938	41	(C20-H39)	1.0955
10	(N4-C6)	1.4781	26	(C11-H31)	1.0846	42	(C21-H40)	1.0924
11	(N4-H26)	1.0132	27	(C12-H32)	1.0852	43	(C21-H41)	1.0929
12	(C5-C6)	1.5575	28	(C13-C14)	1.3975	44	(C21-H42)	1.0956
13	(C5-C22)	1.5268	29	(C13-C15)	1.4003	45	(C22-H43)	1.0893
14	(C5-H27)	1.0984	30	(C14-C16)	1.3931	46	(C22-H44)	1.0935
15	(C6-C13)	1.5327	31	(C14-H33)	1.0816	47	(C22-H45)	1.0916
16	(C6-H28)	1.0956	32	(C15-C17)	1.3962			

H26 = 109.743º] indicate a pyramidal geometry. Among all the bond angles, the largest was observed for C6–C13–C14 (124.751º), while the smallest was found for C6–C5–H27 (103.262º). The complete geometrical parameters of the title compound are summarized in Table-3.

Dihedral angle interpretation: The geometric relationship between the two portions of a molecule connected by a chemical bond is represented by a torsion angle, which is a specific example of a dihedral angle in stereochemistry [36]. A half-plane is defined by each set of three non-colinear atoms in a molecule. As previously mentioned, a dihedral angle is formed when two of these half-planes (*i.e.* a group of four consecutively bonded atoms) cross. It is possible to describe the molecule conformation through dihedral angles. The two sorts of words that may be used to define four ranges of angles include the following: stereochemical arrangements

TABLE-3
BOND ANGLE VALUES OF THE OPTIMIZED GEOMETRY OF MBMP MOLECULE

S. No.	Atom set	Bond angle (°)	S. No.	Atom set	Bond angle (°)	S. No.	Atom set	Bond angle (°)
1	(C2-C1-C3)	112.285	29	(C5-C6-H28)	105.288	57	(C17-C15-H34)	118.626
2	(C2-C1-H23)	107.113	30	(C13-C6-H28)	105.161	58	(C14-C16-C18)	120.712
3	(C2-C1-H24)	112.207	31	(C2-C7-C8)	123.777	59	(C14-C16-H35)	119.517
4	(C3-C1-H23)	107.117	32	(C2-C7-C9)	117.966	60	(C18-C16-H35)	119.770
5	(C3-C1-H24)	109.683	33	(C8-C7-C9)	118.192	61	(C15-C17-C18)	118.052
6	(H23-C1-H24)	108.193	34	(C7-C8-C10)	121.848	62	(C15-C17-C21)	120.992
7	(C1-C2-N4)	107.843	35	(C7-C8-H29)	120.073	63	(C18-C17-C21)	120.954
8	(C1-C2-C7)	114.710	36	(C10-C8-H29)	118.076	64	(C16-C18-C17)	120.390
9	(C1-C2-H25)	106.583	37	(C7-C9-C11)	120.789	65	(C16-C18-H36)	119.913
10	(N4-C2-C7)	116.860	38	(C7-C9-H30)	119.878	66	(C17-C18-H36)	119.694
11	(N4-C2-H25)	104.564	39	(C11-C9-H30)	119.325	67	(C10-C20-H37)	111.460
12	(C7-C2-H25)	105.275	40	(C8-C10-C12)	118.612	68	(C10-C20-H38)	111.389
13	(C1-C3-C5)	113.882	41	(C8-C10-C20)	120.341	69	(C10-C20-H39)	110.981
14	(C1-C3-O19)	122.705	42	(C12-C10-C20)	121.038	70	(H37-C20-H38)	108.142
15	(C5-C3-O19)	123.403	43	(C9-C11-C12)	120.159	71	(H37-C20-H39)	107.193
16	(C2-N4-C6)	119.725	44	(C9-C11-H31)	119.941	72	(H38-C20-H39)	107.480
17	(C2-N4-H26)	110.423	45	(C12-C11-H31)	119.897	73	(C17-C21-H40)	111.428
18	(C6-N4-H26)	109.743	46	(C10-C12-C11)	120.396	74	(C17-C21-H41)	111.409
19	(C3-C5-C6)	110.846	47	(C10-C12-H32)	119.735	75	(C17-C21-H42)	111.049
20	(C3-C5-C22)	113.829	48	(C11-C12-H32)	119.867	76	(H40-C21-H41)	108.011
21	(C3-C5-H27)	104.074	49	(C6-C13-C14)	124.751	77	(H40-C21-H42)	107.476
22	(C6-C5-C22)	115.042	50	(C6-C13-C15)	117.156	78	(H41-C21-H42)	107.271
23	(C6-C5-H27)	103.262	51	(C14-C13-C15)	118.090	79	(C5-C22-H43)	112.194
24	(C22-C5-H27)	108.601	52	(C13-C14-C16)	120.227	80	(C5-C22-H44)	110.363
25	(N4-C6-C5)	108.288	53	(C13-C14-H33)	120.713	81	(C5-C22-H45)	110.151
26	(N4-C6-C13)	115.824	54	(C16-C14-H33)	119.056	82	(H43-C22-H44)	108.157
27	(N4-C6-H28)	104.278	55	(C13-C15-C17)	122.523	83	(H43-C22-H45)	107.524
28	(C5-C6-C13)	116.654	56	(C13-C15-H34)	118.848	84	(H44-C22-H45)	108.324

TABLE-4
DIHEDRAL ANGLE VALUES OF MBMP MOLECULE (OPTIMISED GEOMETRY)

S.No.	Atom set	Dihedral angle (°)	Conformation	S.No.	Atom set	Dihedral angle (°)	Conformation
1	(C3-C1-C2-N4)	50.1	+sc	63	(H28-C6-C13-C15)	30.6	+sc
2	(C3-C1-C2-C7)	-82.0	-sc	64	(C2-C7-C8-C10)	-177.7	-ap
3	(C3-C1-C2-H25)	161.9	+ap	65	(C2-C7-C8-H29)	3.0	+sp
4	(H23-C1-C2-N4)	-67.2	-sc	66	(C9-C7-C8-C10)	-0.7	-sp
5	(H23-C1-C2-C7)	160.6	+ap	67	(C9-C7-C8-H29)	180.0	+ap
6	(H23-C1-C2-H25)	44.6	+sc	68	(C2-C7-C9-C11)	177.8	+ap
7	(H24-C1-C2-N4)	174.2	+ap	69	(C2-C7-C9-H30)	-1.2	-sp
8	(H24-C1-C2-C7)	42.1	+sc	70	(C8-C7-C9-C11)	0.6	+sp
9	(H24-C1-C2-H25)	-74.0	-sc	71	(C8-C7-C9-H30)	-178.4	-ap
10	(C2-C1-C3-C5)	-52.9	-sc	72	(C7-C8-C10-C12)	0.4	+sp
11	(C2-C1-C3-O19)	128.2	+ac	73	(C7-C8-C10-C20)	-178.5	-ap
12	(H23-C1-C3-C5)	64.4	+sc	74	(H29-C8-C10-C12)	179.7	+ap
13	(H23-C1-C3-O19)	-114.5	-ac	75	(H29-C8-C10-C20)	0.9	+sp
14	(H24-C1-C3-C5)	-178.4	-ap	76	(C7-C9-C11-C12)	-0.3	-sp
15	(H24-C1-C3-O19)	2.7	+sp	77	(C7-C9-C11-H31)	-179.6	-ap
16	(C1-C2-N4-C6)	-55.4	-sc	78	(H30-C9-C11-C12)	178.7	+ap
17	(C1-C2-N4-H26)	175.8	+ap	79	(H30-C9-C11-H31)	-0.6	-sp
18	(C7-C2-N4-C6)	75.6	+sc	80	(C8-C10-C12-C11)	0.0	-sp
19	(C7-C2-N4-H26)	-53.3	-sc	81	(C8-C10-C12-H32)	179.5	+ap
20	(H25-C2-N4-C6)	-168.5	-ap	82	(C20-C10-C12-C11)	178.9	+ap
21	(H25-C2-N4-H26)	62.6	+sc	83	(C20-C10-C12-H32)	-1.6	-sp
22	(C1-C2-C7-C8)	5.9	+sp	84	(C8-C10-C20-H37)	-37.5	-sc
23	(C1-C2-C7-C9)	-171.1	-ap	85	(C8-C10-C20-H38)	-158.4	-ap
24	(N4-C2-C7-C8)	-121.8	-ac	86	(C8-C10-C20-H39)	81.9	+sc
25	(N4-C2-C7-C9)	61.2	+sc	87	(C12-C10-C20-H37)	143.6	+ac
26	(H25-C2-C7-C8)	122.7	+ac	88	(C12-C10-C20-H38)	22.8	+sp
27	(H25-C2-C7-C9)	-54.3	-sc	89	(C12-C10-C20-H39)	-97.0	-ac
28	(C1-C3-C5-C6)	52.6	+sc	90	(C9-C11-C12-C10)	0.0	-sp
29	(C1-C3-C5-C22)	-175.9	-ap	91	(C9-C11-C12-H32)	-179.6	-ap
30	(C1-C3-C5-H27)	-57.8	-sc	92	(H31-C11-C12-C10)	179.3	+ap
31	(O19-C3-C5-C6)	-128.5	-ac	93	(H31-C11-C12-H32)	-0.3	-sp
32	(O19-C3-C5-C22)	3.0	+sp	94	(C6-C13-C14-C16)	-178.8	-ap
33	(O19-C3-C5-H27)	121.1	+ac	95	(C6-C13-C14-H33)	1.9	+sp
34	(C2-N4-C6-C5)	56.0	+sc	96	(C15-C13-C14-C16)	0.5	+sp
35	(C2-N4-C6-C13)	-77.3	-sc	97	(C15-C13-C14-H33)	-178.8	-ap
36	(C2-N4-C6-H28)	167.7	+ap	98	(C6-C13-C15-C17)	178.4	+ap
37	(H26-N4-C6-C5)	-174.9	-ap	99	(C6-C13-C15-H34)	-2.3	-sp
38	(H26-N4-C6-C13)	51.9	+sc	100	(C14-C13-C15-C17)	-1.0	-sp
39	(H26-N4-C6-H28)	-63.1	-sc	101	(C14-C13-C15-H34)	178.3	+ap
40	(C3-C5-C6-N4)	-50.4	-sc	102	(C13-C14-C16-C18)	0.1	+sp
41	(C3-C5-C6-C13)	82.4	+sc	103	(C13-C14-C16-H35)	-179.5	-ap
42	(C3-C5-C6-H28)	-161.5	-ap	104	(H33-C14-C16-C18)	179.4	+ap
43	(C22-C5-C6-N4)	178.7	+ap	105	(H33-C14-C16-H35)	-0.2	-sp
44	(C22-C5-C6-C13)	-48.5	-sc	106	(C13-C15-C17-C18)	0.8	+sp
45	(C22-C5-C6-H28)	67.6	+sc	107	(C13-C15-C17-C21)	-178.6	-ap
46	(H27-C5-C6-N4)	60.5	+sc	108	(H34-C15-C17-C18)	-178.5	-ap
47	(H27-C5-C6-C13)	-166.7	-ap	109	(H34-C15-C17-C21)	2.0	+sp
48	(H27-C5-C6-H28)	-50.5	-sc	110	(C14-C16-C18-C17)	-0.3	-sp
49	(C3-C5-C22-H43)	-61.2	-sc	111	(C14-C16-C18-H36)	-179.7	-ap
50	(C3-C5-C22-H44)	178.1	+ap	112	(H35-C16-C18-C17)	179.3	+ap
51	(C3-C5-C22-H45)	58.6	+sc	113	(H35-C16-C18-H36)	-0.1	-sp
52	(C6-C5-C22-H43)	68.3	+sc	114	(C15-C17-C18-C16)	-0.1	-sp
53	(C6-C5-C22-H44)	-52.4	-sc	115	(C15-C17-C18-H36)	179.3	+ap
54	(C6-C5-C22-H45)	-172.0	-ap	116	(C21-C17-C18-C16)	179.3	+ap
55	(H27-C5-C22-H43)	-176.6	-ap	117	(C21-C17-C18-H36)	-1.3	-sp
56	(H27-C5-C22-H44)	62.7	+sc	118	(C15-C17-C21-H40)	-23.0	-sp
57	(H27-C5-C22-H45)	-56.8	-sc	119	(C15-C17-C21-H41)	-143.7	-ac
58	(C4-C6-C13-C14)	95.5	+ac	120	(C15-C17-C21-H42)	96.8	+ac
59	(C4-C6-C13-C15)	-83.9	-sc	121	(C18-C17-C21-H40)	157.6	+ap
60	(C5-C6-C13-C14)	-33.8	-sc	122	(C18-C17-C21-H41)	36.9	+sc
61	(C5-C6-C13-C15)	146.8	+ac	123	(C18-C17-C21-H42)	-82.6	-sc
62	(H28-C6-C13-C14)	-150.0	-ap				

corresponding to angles, (i) 0º to ± 30º *syn*-periplanar (sp); (ii) 30º to 90º and -30º to -90º *syn*-clinal (sc); (iii) 90º to 150º and -90º to -150º *anti*-clinal (ac), and (iv) ±150º to 180º *anti*-periplanar (ap).

The *syn*-periplanar conformation is also referred to as the *cis*- or *syn*-conformation, while the anti-periplanar corresponds to the trans conformation. Similarly, the *syn*-clinal is known as the *gauche* or *skew* form, and the anti-clinal represents an intermediate arrangement. As shown in Table-4, the target molecule exhibits a combination of *syn*-periplanar (sp), *anti*-periplanar (ap), *anti*-clinal (ac) and *syn*-clinal (sc) conformations.

According to the computed dihedral angles C3–C1–C2–N4 (50.1º) and C1–C2–N4–C6 (-55.4º) [37], the piperidone ring favoured adopting the chair configuration. The dihedral angles of C5–C4–N1–H1 and C3–C2–N1–H1 show slight variations, likely due to weak interactions with neighbouring atoms. Among the possible conformations, the piperidone ring predominantly adopts the more stable chair form. In this arrangement, the N–H group is favourably oriented near the equatorial position, contributing to its stability [38,39]. The calculated dihedral angle values in this study are in close agreement with those reported in the literature by Ramalingam *et al.* [40].

Mulliken charges: Mulliken charge analysis provides insight into the distribution of electronic charge within a molecule by equally partitioning orbital overlap among atoms [41]. This charge distribution influences bond lengths and is crucial in determining properties such as dipole moment, polarisability, chemical reactivity and acid-base behaviour, making it an important parameter in quantum chemical studies [42,43]. It is revealed from the results that the nitrogen atom N4 (-0.374 a.u.) in the piperidone ring has a strong negative charge. All carbon atoms are negatively charged except C3 (0.229 a.u.), which is attached to the O19 atom (Fig. 2). The results indicate that the H26 atom (0.192 a.u.), attached to the ring nitrogen (N12), carries a higher positive charge than the other hydrogen atoms in MBMP, likely due to its involvement in intramolecular hydrogen bonding (Table-5). This highlights charge transfer interactions and helps identify the potential reactive sites within the molecule (Fig. 3). Furthermore, the charge distribution on key atoms plays a significant role in determining the molecule's bonding ability.

TABLE-5
MULLIKEN CHARGE VALUES OF MBMP MOLECULE

Atom No.	Mulliken charge (a.u.)	Atom No.	Mulliken charge (a.u.)	Atom No.	Mulliken charge (a.u.)
C1	-0.225	C16	-0.090	H31	0.088
C2	-0.067	C17	-0.096	H32	0.080
C3	0.229	C18	-0.070	H33	0.108
N4	-0.374	O19	-0.310	H34	0.068
C5	-0.233	C20	-0.258	H35	0.090
C6	-0.047	C21	-0.259	H36	0.080
C7	-0.016	C22	-0.223	H37	0.118
C8	-0.084	H23	0.137	H38	0.108
C9	-0.070	H24	0.144	H39	0.126
C10	-0.101	H25	0.140	H40	0.108
C11	-0.084	H26	0.192	H41	0.115
C12	-0.067	H27	0.140	H42	0.125
C13	-0.024	H28	0.133	H43	0.119
C14	-0.071	H29	0.102	H44	0.101
C15	-0.066	H30	0.070	H45	0.112

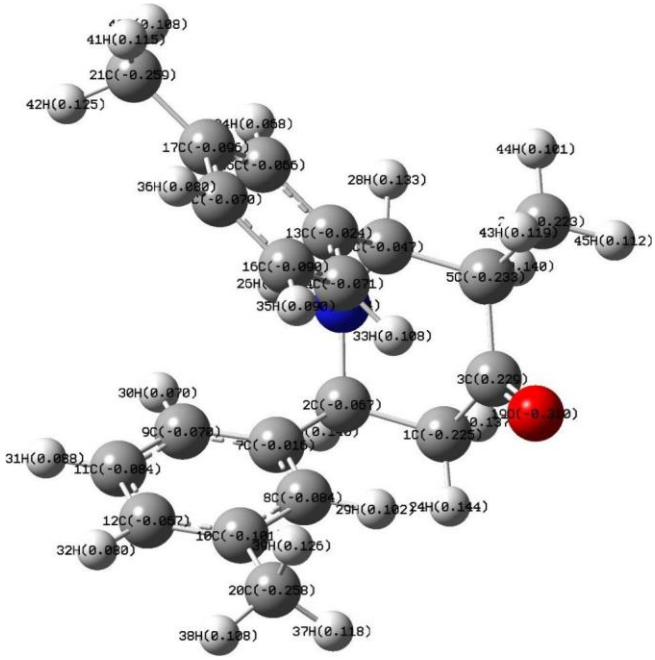

Fig. 3. Mulliken atomic charge distribution of MBMP molecule

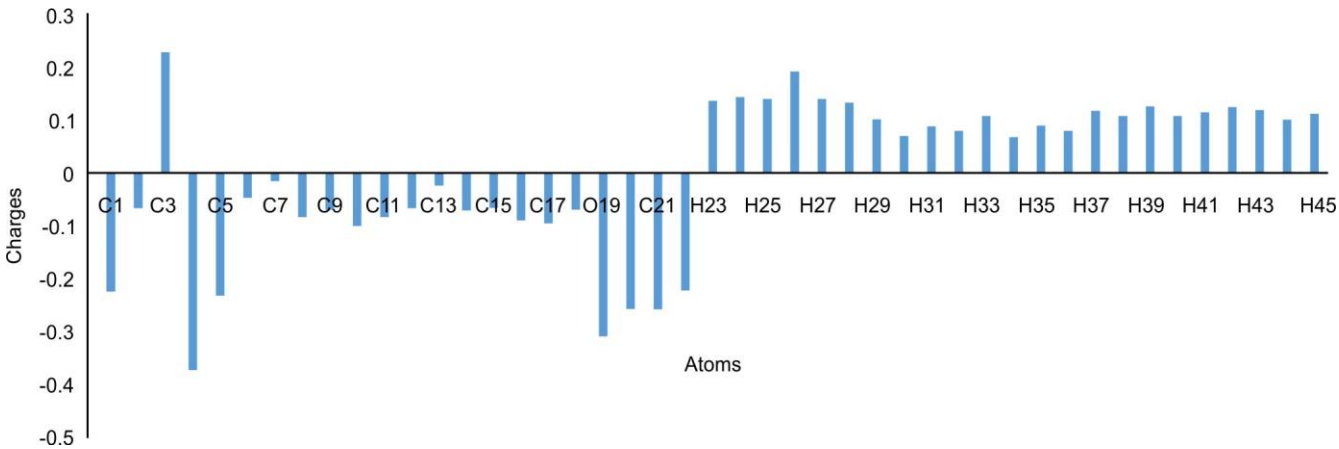

Fig. 2. Mulliken atomic charge chart of 3-methyl-2,6-*bis*(3-methylphenyl)piperidin-4-one (MBMP) molecule

Molecular electrostatic potential (MEP) analysis: MEP analysis is widely used to examine reactive sites and intermolecular interactions within a molecule [44,45]. It helps distinguish electrophilic and nucleophilic regions, which are important for understanding biological activity and interaction behaviour [46-48]. In the MEP map, negative regions (red) indicate electron-rich sites prone to electrophilic attack, while the positive regions (blue) represent electron-deficient areas susceptible to nucleophilic interaction; green regions correspond to near-neutral potential.

For the target molecule, the carbonyl oxygen exhibits a negative potential region, whereas the area around the nitrogen and attached hydrogen atoms shows positive potential. The presence of intermediate green regions reflects a balanced distribution between these extremes. Such charge distribution provides valuable insight into potential reactive sites (Fig. 4) and is useful for predicting drug–receptor and enzyme–substrate interactions [49,50].

Frontier molecular orbitals (FMO) and quantum chemical calculations: In this study, HOMO is mainly distributed over the molecular ring system, while LUMO is localized on the ring and sp^2-hybridized atoms such as nitrogen, oxygen and aromatic carbons. The HOMO–LUMO energies were calculated using the same level of theory to evaluate the electronic behaviour of the molecule. The investigated molecule has HOMO and LUMO values of -6.206 eV and -0.864 eV, respectively. It is determined that the energy gap (ΔE) is 5.342 eV. The stability of the title molecule is demonstrated by this wide gap. The HOMO and LUMO distributions of the MBMP molecule were obtained based on the optimized geometry at the B3LYP/6-311G(d,p) level, as shown in Fig. 5a-b. The HOMO energy is related to the ionisation potential (I), while the LUMO energy corresponds to the electron affinity (A) of the molecule [51]. Using these energies, global reactivity parameters such as electronegativity (χ), chemical potential (μ), electrophilicity index (ω), hardness (η) and softness (S) were calculated [52,53]. The results (Table-6) indicate that the title molecule exhibits stronger electron donating ability than electron-accepting character, and the higher hardness value compared to softness suggests that MBMP behaves as a relatively hard molecule.

Fukui function analysis: In this study, Fukui functions for electrophilic, nucleophilic and free radical attacks were calculated using the same level of theory, enabling the identification of reactive regions within the molecule [54,55]. The formulae used are as follows [56]:

For electrophilic attack:

$$f_j^- = q_j(N) - q_j(N-1) \quad (1)$$

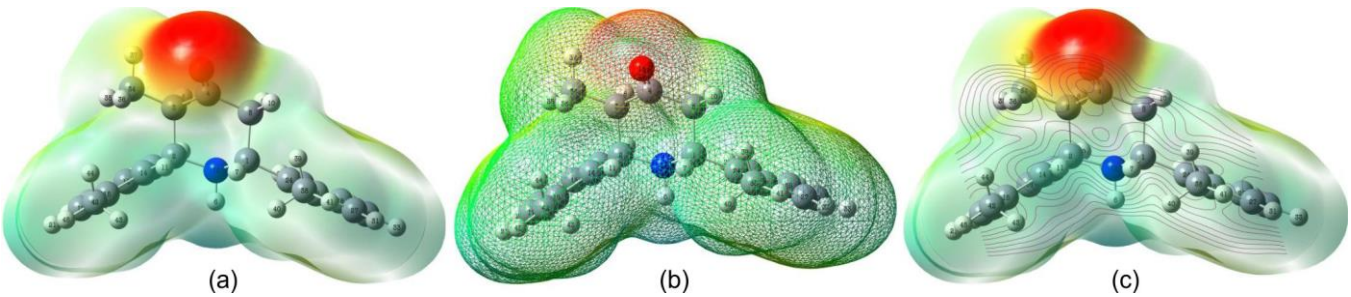

Fig. 4. The MEP image of (a) transparent, (b) Mesh format and (c) contour diagram of MBMP molecule

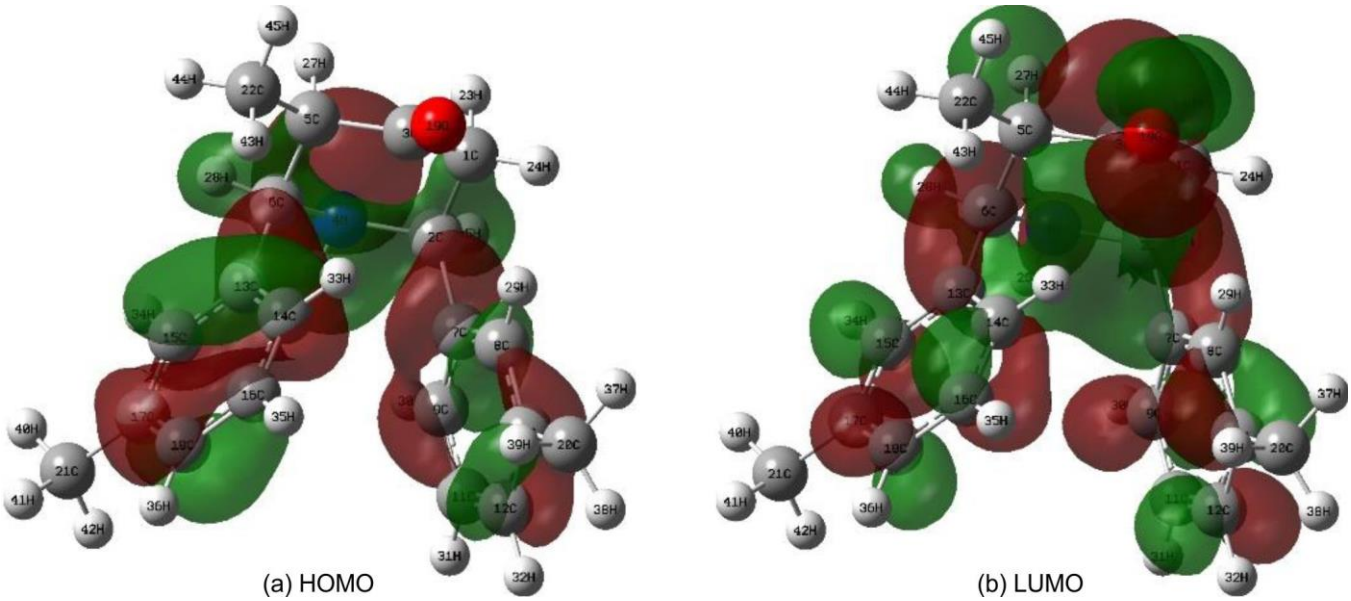

Fig. 5. HOMO-LUMO cloud distributions of MBMP molecule

TABLE-6
IDENTIFIED REACTIVE PARAMETERS
OF THE MBMP MOLECULE

Quantum chemical parameters	Charge (eV)
E_{LUMO}	-0.864
E_{HOMO}	-6.206
Energy band gap $\Delta E = E_{HOMO} - E_{LUMO}$	5.342
Ionization potential $I = -E_{HOMO}$	6.206
Electron affinity $A = -E_{LUMO}$	0.864
Chemical hardness $\eta = I-A/2$	2.671
Global softness $s = 1/2\eta$	0.187
Electronegativity $\chi = I+A/2$	3.535
Chemical potential $\mu = -I+A/2$	-3.535
Electrophilicity index $\omega = \mu^2/2\eta$	2.339
Electron accepting $\omega^+ = I+3A2/16I-A$	0.906
Donating capability $\omega^- = 3I+A2/16I-A$	4.440
Chemical softness $\sigma = 1/\eta$	0.374
Optical softness $\sigma_0 = 1/\Delta E$	0.187
Nucleophilicity index $N = 1/\omega$	0.428
Additional electronic charges $\Delta N_{max} = -\mu/\eta$	1.323

For nucleophilic attack:

$$f_j^+ = q_j(N+1) - q_j(N) \quad (2)$$

For free radical attack:

$$f_j^0 = \frac{1}{2}\left[q_j(N+1) - q_j(N-1)\right] \quad (3)$$

here, q_j is the atomic charge at the j^{th} atomic site, (N), (N+1) and (N-1) are the total electrons present in the neutral, anionic and cationic states of the studied molecule, respectively [57]. The dual descriptor Δf(r) is defined as the difference between the electrophilic and nucleophilic Fukui functions, providing a clearer identification of reactive sites within the molecule. This approach, introduced by Morell *et al*. [58], allows the simultaneous evaluation of regions susceptible to both types of chemical attack and defined as follows:

$$\Delta f(r) = \left[f_j^+ - f_j^-\right] \quad (4)$$

This description states that if Δf(r) < 0, a site is susceptible to electrophilic attack and if Δf(r) > 0, it is susceptible to nucleophilic attack.

The reactivity of MBMP was analysed using NPA, MPA and dual descriptor (Δf(r)) approaches, as summarized in Table-7. The NPA results indicate that the nitrogen atom (N4) is the most favourable site for electrophilic attack across anionic, cationic and neutral species, while the carbon atom (C3) is predominantly susceptible to nucleophilic attack. Similarly, MPA analysis highlights oxygen (O19) and nitrogen (N4) as key electrophilic centers, with hydrogen (H26) and carbon (C3) contributing to nucleophilic regions.

The order of reactive sites varies slightly depending on the molecular charge state; however, nitrogen (N4), oxygen (O19) and certain carbon atoms consistently emerge as major reactive centers. The dual descriptor (Δf(r)) further supports these findings, where atoms such as C2, C3, C6, C10, C11, C16, C17, C20, C21, C22, H26 and H29 exhibit negative values, indicating susceptibility to electrophilic attack, while atoms with positive values are more prone to nucleophilic attack. These combined analyses provide a clear understanding of the charge distribution and reactive regions within the molecule, as illustrated in Fig. 6.

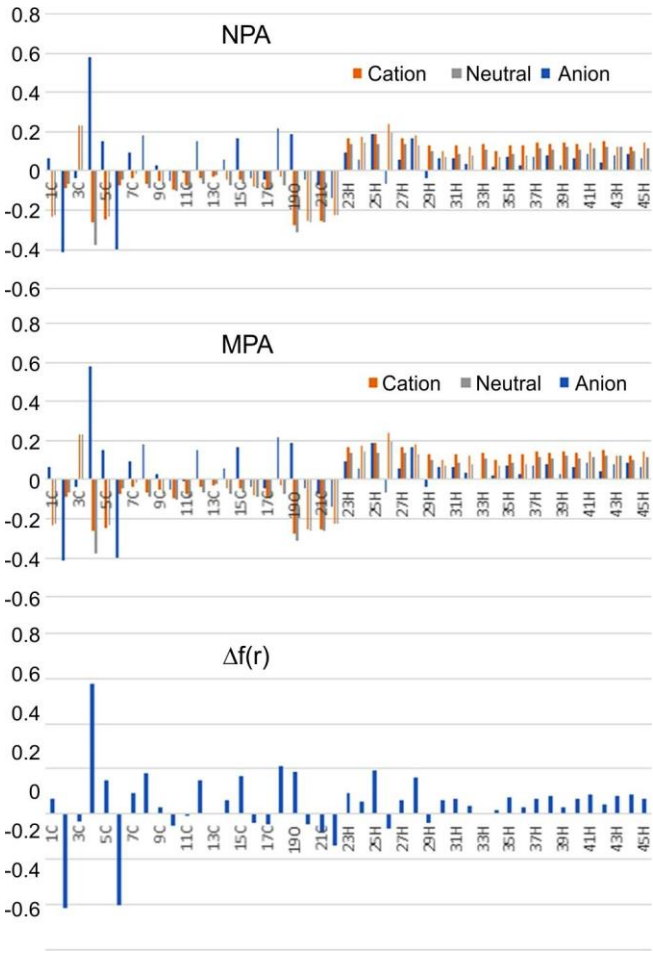

Fig. 6. NPA, MPA and Δf(r) representations of the MBMP molecule

Natural bond order (NBO) analysis: Natural bond orbital (NBO) analysis is used to study intra- and intermolecular interactions by examining electron density distribution and charge transfer between donor and acceptor orbitals [59-61]. It is particularly useful for understanding hydrogen bonding, where hyperconjugative interactions influence bond strength and geometry [62]. The extent of charge transfer affects the elongation or contraction of X–H bonds, and the associated stabilization energy E(2) was calculated using eqn. 5 [63-66]:

$$E(2) = \Delta E_{ij} = q_i \frac{F(i,j)^2}{E_j - E_i} \quad (5)$$

where q_i is the donor orbital occupancy, E_j is the diagonal elements and F(i,j) is the off-diagonal NBO Fock matrix element. The more strongly the donor and electron acceptor are connected, the more likely the donor is to donate to the acceptor; also, the more conjugated the system as a whole, the higher the E(2) value. A few NBO analytical findings for the chemical under study are summarised in Table-8.

NBO analysis reveals significant donor-acceptor interactions contributing to the stabilization of the MBMP molecule. The σ(C1-H23)→π*(C3-O19) interaction provides a stabilization energy of 6.12 kcal/mol, while σ(C2-H25)→σ*(N4-C6)

TABLE-7
NPA AND MPA VALUES WITH Δf(r) FOR THE CATIONIC, ANIONIC AND NEUTRAL FORMS OF MBMP MOLECULE

Atom	NPA (a.u.)				MPA (a.u.)		
	f_j^-	f_j^+	f_j^0	Δf(r)	$Q_{(N-1)}$	$Q_{(N+1)}$	$Q_{(N0)}$
1C	-0.4379	-0.3727	-0.5135	0.0652	-0.2004	-0.2304	-0.2246
2C	0.6065	0.1913	0.5516	-0.4152	-0.0599	-0.0874	-0.0668
3C	0.6083	0.5728	0.6812	-0.0355	0.1505	0.2323	0.2295
4N	-1.0270	-0.4488	-0.9585	0.5782	-0.3657	-0.2598	-0.3743
5C	-0.1557	-0.0069	-0.2014	0.1488	-0.1956	-0.2483	-0.2332
6C	0.4540	0.0531	0.3846	-0.4009	-0.0379	-0.0715	-0.0467
7C	-0.1069	-0.0115	-0.1755	0.0954	-0.0209	-0.0331	-0.0161
8C	-0.3650	-0.1865	-0.2326	0.1785	-0.0782	-0.0675	-0.0840
9C	-0.1744	-0.1439	-0.1014	0.0305	-0.0924	-0.0487	-0.0698
10C	0.3443	0.2917	0.2850	-0.0526	-0.1068	-0.0972	-0.1005
11C	-0.0894	-0.0914	-0.1164	-0.002	-0.0866	-0.0703	-0.0841
12C	-0.3637	-0.2143	-0.2548	0.1494	-0.1022	-0.0399	-0.0670
13C	0.1234	0.1247	0.0336	0.0013	-0.0271	-0.0282	-0.0237
14C	-0.0397	0.0214	0.0070	0.0611	-0.0599	-0.0454	-0.0705
15C	-0.5675	-0.3984	-0.4351	0.1691	-0.0993	-0.0472	-0.0665
16C	-0.1887	-0.2247	-0.1930	-0.036	-0.1133	-0.0834	-0.0902
17C	0.3936	0.3473	0.3563	-0.0463	-0.0805	-0.0962	-0.0956
18C	-0.3614	-0.1480	-0.2705	0.2134	-0.1057	-0.0263	-0.0701
19O	-0.6349	-0.4479	-0.5034	0.187	-0.4040	-0.2737	-0.3096
20C	-0.4250	-0.4679	-0.4461	-0.0429	-0.2578	-0.2522	-0.2577
21C	-0.3918	-0.4669	-0.4302	-0.0751	-0.2630	-0.2525	-0.2586
22C	-0.2852	-0.4247	-0.3077	-0.1395	-0.2267	-0.2221	-0.2231
23H	0.0475	0.1386	0.1376	0.0911	0.0701	0.1694	0.1373
24H	0.0782	0.1349	0.1215	0.0567	0.1017	0.1751	0.1437
25H	-0.0822	0.1086	0.0171	0.1908	0.0658	0.1871	0.1400
26H	0.3913	0.3254	0.3910	-0.0659	0.1737	0.2404	0.1918
27H	0.0288	0.0875	0.1014	0.0587	0.0812	0.1676	0.1396
28H	-0.0431	0.1212	0.0425	0.1643	0.0691	0.1812	0.1333
29H	0.1727	0.1353	0.1462	-0.0374	0.0899	0.1275	0.1016
30H	0.0724	0.1368	0.0936	0.0644	0.0363	0.1043	0.0699
31H	0.0911	0.1573	0.1242	0.0662	0.0476	0.1286	0.0880
32H	0.1276	0.1671	0.1452	0.0395	0.0359	0.1214	0.0797
33H	0.0991	0.1062	0.0998	0.0071	0.1071	0.1378	0.1085
34H	0.1579	0.1773	0.1621	0.0194	0.0351	0.1019	0.0685
35H	0.1083	0.1801	0.1394	0.0718	0.0543	0.1282	0.0897
36H	0.1337	0.1649	0.1533	0.0312	0.0367	0.1276	0.0804
37H	0.0918	0.1610	0.1220	0.0692	0.0975	0.1447	0.1175
38H	0.0776	0.1573	0.1169	0.0797	0.0759	0.1383	0.1076
39H	0.1163	0.1456	0.1297	0.0293	0.1125	0.1475	0.1256
40H	0.0899	0.1568	0.1189	0.0669	0.0880	0.1338	0.1079
41H	0.0672	0.1541	0.1082	0.0869	0.0890	0.1442	0.1149
42H	0.1005	0.1451	0.1213	0.0446	0.1057	0.1525	0.1252
43H	0.0333	0.1159	0.0593	0.0826	0.1051	0.1244	0.1194
44H	0.0399	0.1254	0.0809	0.0855	0.0712	0.1219	0.1013
45H	0.0844	0.1501	0.1086	0.0657	0.0840	0.1440	0.1120

contributes 5.00 kcal/mol. Similarly, σ(C5-H27)→π*(C3-O19) interaction shows a stabilization of 6.39 kcal/mol. Strong π-π* interactions are observed within the aromatic systems, where π(C7-C8)→π*(C9-C11) and π(C9-C8)→π*(C9-C11) contribute 19.29 and 21.04 kcal/mol, respectively. Additional stabilisation arises from π(C7-C8)→π*(C10-C12) (21.89 kcal/mol) and π(C10-C12)→π*(C7-C8) (19.09 kcal/mol), along with π(C9-C11)→π*(C10-C12) (18.40 kcal/mol) and the reverse interaction (22.05 kcal/mol).

Further π–π* interactions involving aromatic rings, such as π(C13–C14), π(C15–C17) and π(C16–C18), contribute stabilization energies in the range of ~19-22 kcal/mol, indicating strong electron delocalization. In addition, lone pair interactions play a crucial role, where LP(2)O19 donates to σ*(C3–C5) and σ*(C1–C3) with stabilization energies of 20.79 and 20.18 kcal/mol, respectively. The LP(1)N4 also contributes to stabilization *via* σ*(C2–C7) and σ*(C6–C13) interactions with energies of 8.84 and 8.44 kcal/mol. These interactions collect-

TABLE-8
NBO RELATED PARAMETERS VALUES OF MBMP MOLECULE

Type	Donor NBO	ED/e (a.u.)	Type	Acceptor NBO	ED/e (a.u.)	E(2)[a] (kcal/mol)	E(j)-E(i)[b]	F(i,j)[c]
σ	C1-H23	1.9567	π*	C3-O19	0.0950	6.12	0.52	0.051
σ	C2-H25	1.9597	σ*	N4-C6	0.0336	5.00	0.83	0.058
σ	C5-H27	1.9432	π*	C3-O19	0.0950	6.39	0.50	0.051
π	C7-C8	1.6677	π*	C9-C11	0.3258	19.29	0.28	0.066
π	C7-C8	1.6677	π*	C10-C12	0.3362	21.89	0.29	0.071
π	C9-C11	1.6827	π*	C7-C8	0.3375	21.04	0.29	0.070
π	C9-C11	1.6827	π*	C10-C12	0.3362	18.40	0.29	0.066
π	C10-C12	1.6550	π*	C7-C8	0.3375	19.09	0.29	0.066
π	C10-C12	1.6550	π*	C9-C11	0.3258	22.05	0.28	0.071
π	C13-C14	1.6509	π*	C15-C17	0.3459	19.65	0.29	0.067
π	C13-C14	1.6509	π*	C16-C18	0.3294	21.49	0.28	0.070
π	C15-C17	1.6571	π*	C13-C14	0.3509	21.94	0.29	0.071
π	C15-C17	1.6571	π*	C16-C18	0.3294	19.23	0.28	0.066
π	C16-C18	1.6690	π*	C13-C14	0.3509	19.51	0.29	0.067
π	C16-C18	1.6690	π*	C15-C17	0.3459	21.93	0.29	0.071
LP(2)	O19	1.8895	σ*	C3-C5	0.0736	20.79	0.66	0.106
LP(2)	O19	1.8895	σ*	C1-C3	0.0617	20.18	0.66	0.104
LP(1)	N4	1.9055	σ*	C2-C7	0.0479	8.84	0.68	0.070
LP(1)	N4	1.9055	σ*	C6-C13	0.0466	8.44	0.69	0.069

[a]E(2) means energy of hyperconjugative interactions (stabilisation energy). ED/e means the electron density. [b]Energy difference between donor and acceptor i and j NBO orbitals. [c]F(i, j) is the Fock matrix element between i and j NBO orbital. LP(n)A is a valence lone pair orbital (n) on A atom.

ively highlight strong hyperconjugation and electron delocalisation within the molecule, contributing significantly to its overall stability.

Non-covalent interaction (NCI): Non-covalent interactions can be identified directly from electron density, as they exhibit distinct signatures. The reduced density gradient (RDG) method is widely used to analyse different types of NCIs in real space [67-69]. In the DFT framework, RDG is a dimensionless function derived from the electron density gradient, describing deviations from a uniform electron distribution. Eqn. 6 expresses RDG (S), which is calculated as:

$$S = \frac{1}{2(3\pi^2)^{1/3}} \frac{|\nabla\rho(r)|}{\rho(r)^{4/3}} \quad (6)$$

The headline molecule's colour-mapped isosurfaces and matching scatter graphs are displayed in Fig. 7. The electron density times the sign of the second highest eigenvalue of the Hessian matrix (λ_2) yields sign (λ_2)ρ(r). It is a valuable metric for predicting the type of contact. Large negative signs (λ_2)ρ(r) suggest attractive interactions like hydrogen bonding, whereas large positive signs (λ_2)ρ(r) indicate repulsive interactions (steric effect). The sign (λ_2)ρ(r) values are extremely near to zero indicate weak van der Waals interactions. NCI isosurfaces are shown using the following colour-coding scheme: blue denotes attractive interactions, red denotes repulsive interactions and green denotes intermediate interactions. The deeper the colour, the higher the level of interaction.

NCI–RDG analysis was performed using the optimized molecular geometry obtained at the same level of theory with Gaussian 16W. The RDG isosurface map (Fig. 7) highlights different types of non-covalent interactions, where red regions indicate steric repulsion and green regions represent weak van der Waals interactions. The red isosurfaces are mainly localized within the phenyl rings, suggesting steric effects in these regions, while the broad green areas correspond to van der Waals interactions distributed across the molecule.

Aromaticity determinations: The studied molecule contains two aromatic benzene rings, whose aromatic character was evaluated and compared using the same level of theory. The PDI [70], BIRD Aromaticity [71], FLU [72], HOMA [73] and PLR [74] data obtained. Multiwfn 3.8 is employed for these determinations. The outcomes are displayed in Table-9. The FLU (eqn. 7), PDI (eqn. 8), HOMA (eqn. 9), BIRD aromaticity (eqn. 10) and PLR (eqn. 11) aromaticity are defined as follows:

$$FLU = \frac{1}{n}\sum_{A-B}^{ring}\left[\left(\frac{V(B)}{V(A)}\right)^{\alpha}\left(\frac{\delta(A,B)-\delta_{ref}(A,B)}{\delta_{ref}(A,B)}\right)\right]^2 \quad (7)$$

where n is equal to the number of atoms in the ring, δ_{ref} is the reference DI value, which is pre-calculated parameter; α is used to ensure the ratio of atomic valences is greater than one:

$$PDI = \frac{\delta(1,4)+\delta(2,5)+\delta(3,6)}{3} \quad (8)$$

$$HOMA = 1 - \sum_i \frac{\alpha_{i,j}}{N}(R_{ref} - R_{i,j})^2 \quad (9)$$

where N is the total number of the atoms considered, j denotes the atom next to atom i, α and R_{Ref} are pre-calculated constants given in original paper for each type of atomic pair:

$$I = 100\left[1-\left(\frac{V}{V_K}\right)\right] \text{ where } V = \frac{100}{\bar{N}}\sqrt{\frac{\sum_i (N_{i,j}-\bar{N})^2}{n}}; N_{i,j} = \frac{a}{R_{i,j}} - b \quad (10)$$

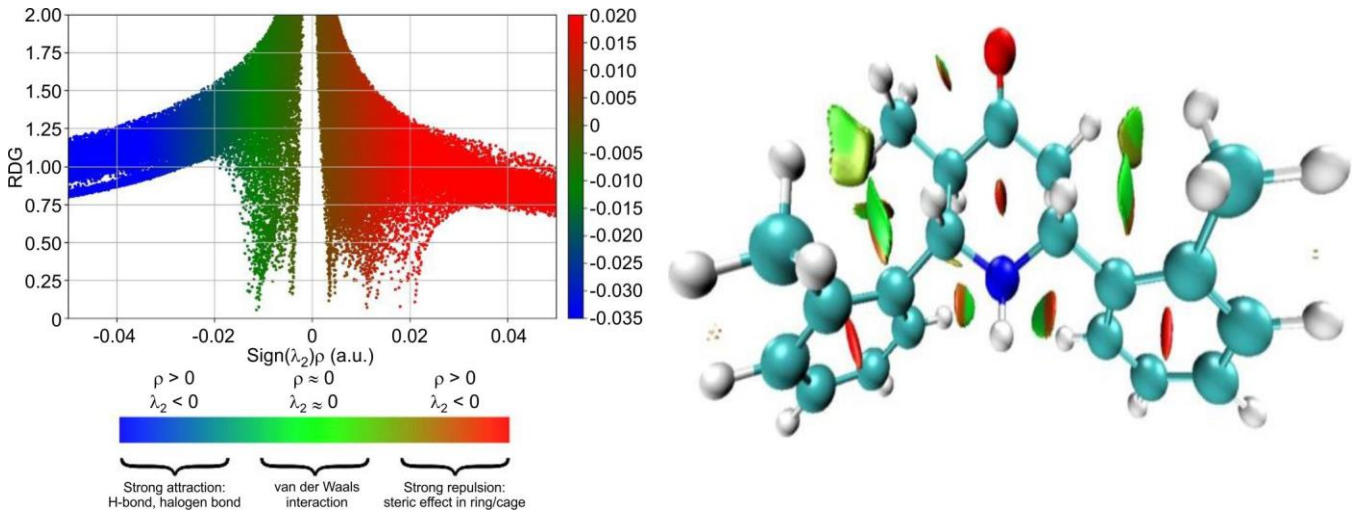

Fig. 7. NCI-RDG isosurfaces and scatter graphs of 3-methyl-2,6-*bis*(3-methylphenyl)piperidin-4-one (MBMP) molecule

TABLE-9
VARIOUS AROMATICITY VALUES DETERMINED OF MBMP MOLECULE

Phenyl ring	PDI	HOMA	BIRD	FLU	PLR
1	0.096921	0.946989	95.512809	0.002134	0.588519
2	0.097074	0.947423	95.476914	0.002171	0.588734

where i cycles over all of the bonds in the ring, j denotes the atom next to atom i. n is the total number of the bonds considered. N denotes Gordy bond order, $\bar{N}$ is the average value of the N values. $R_{i,j}$ is bond length. a and b are predefined parameters, respectively for each type of bonds. V_K is pre-determined reference V:

$$PLR(A,B) = \frac{\chi_{1,4} + \chi_{2,5} + \chi_{3,6}}{3} \quad (11)$$

Table-9 shows the values for PDI, HOMA, BIRD, FLU and PLR aromaticities. The higher the aromatic nature, the lower the FLU number. In this case, ring 1 (with carbon atoms, 14, 15, 16, 17, 18 and 20 as in Fig. 1) of the phenyl is more aromatic than ring 2 (with carbon atoms, 24, 25, 26, 27, 28 and 30 as in Fig. 1). A ring is considered fully aromatic when the HOMA value approaches 1, indicating uniform bond lengths close to the ideal value. Based on the results, phenyl ring 2 shows higher aromaticity than phenyl ring 1. The BIRD index, where values closer to 100 indicate greater aromaticity, also supports this trend. Similarly, PDI, FLU and PLR parameters confirm that phenyl ring 2 is more aromatic than phenyl ring 1.

Simulated scanning tunneling microscope (STM) analysis: The simulated STM image (Fig. 8), generated using Multiwfn 3.8, illustrates spatial variations in tunnelling current at the interface between a conducting surface and a metallic tip [75]. Different values of tip height (Z) and bias voltage (V) were adjusted to obtain optimal images, as shown in Table-10. The maximum local density of states (LDOS) value of 0.114437 a.u. was observed at Z = 0.5 Å and V = -3.5 V. According to the Tersoff-Hamann model, the tunnelling current is directly proportional to LDOS, where brighter regions correspond to higher current intensity. The results indicate that the nitrogen atom of the piperidone ring and selected carbon atoms of the phenyl rings exhibit the highest tunnelling current, reflecting regions of enhanced electronic activity.

TABLE-10
BIAS VOLTAGE AND Z COORDINATES OF XY PLANE ALONG WITH LDOS VALUES OF MBMP MOLECULE

Bias voltage (V)	Z coordinates of XY plane (Å)	LDOS (a.u.)
-3.5	2.2.	0.017541
-3.5	2.0	0.023180
-3.5	1.5	0.055345
-3.5	1.0	0.110450
-3.5	0.5	0.114437
-3.0	0.5	0.076900

Shaded surface map with projection of localised orbital locator (LOL) determinations: According to Schmider & Becke [76], the localised orbital locator (LOL) is a crucial tool for positioning high localisation regions such as the ELF.

$$LOL(r) = \frac{\tau(r)}{1+\tau(r)} \text{ where } (r) = \frac{D_0(r)}{\frac{1}{2}\sum_i \eta_i |\nabla\varphi_i|^2} \quad (12)$$

where $D_0(r)$ for close-shell and spin-polarised systems, which are characterised similarly to ELF, whereas LOL and ELF share a similar relationship. The LOL map of the studied molecule is presented in Fig. 9. The results indicate significant electron localisation around the aromatic rings, highlighting their delocalized π-electron nature. Hydrogen atoms show higher electron density, whereas regions indicated by blue contours represent areas of electron depletion. Moreover, several aromatic carbon atoms exhibit reduced electron density, reflecting charge redistribution within the molecular framework.

UV-Visible studies: The observed UV-Vis spectrum of the title molecule in the range of 200-900 nm is shown in Fig. 10

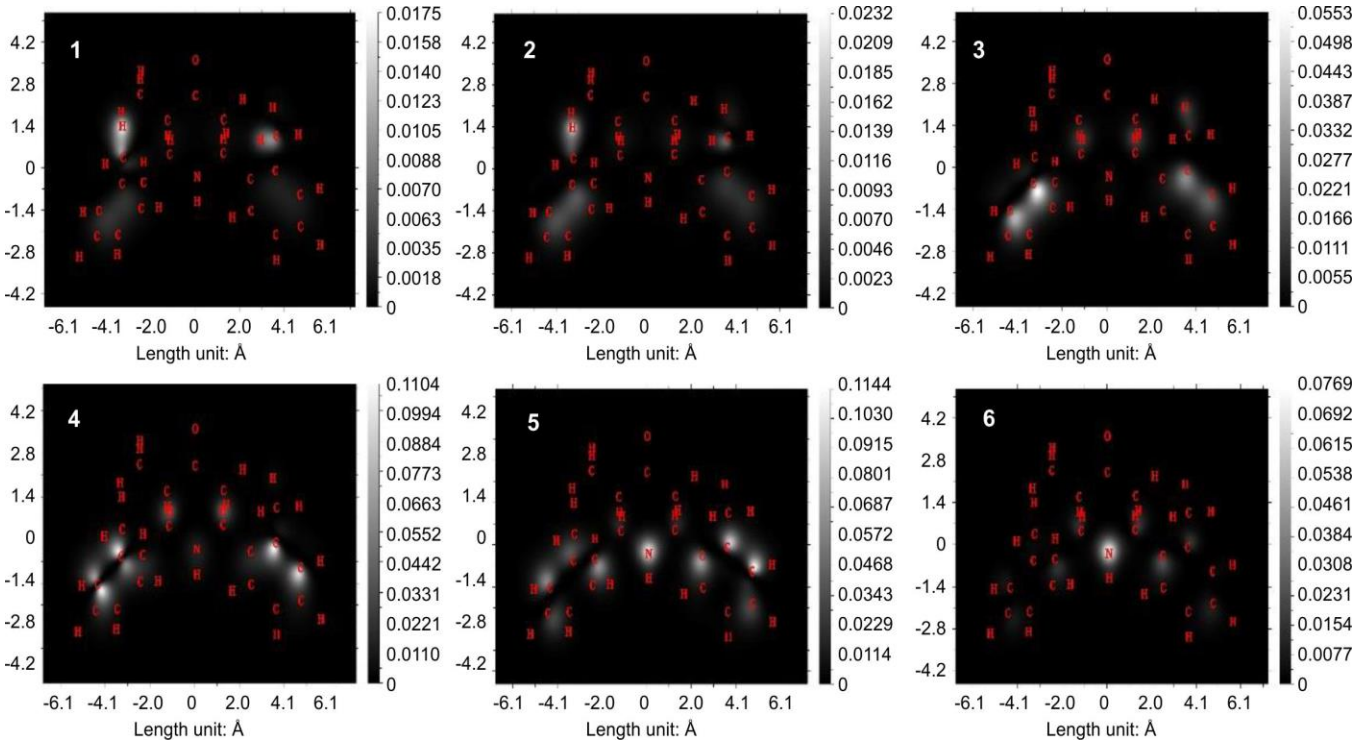

Fig. 8. STM image of 3-methyl-2,6-*bis*(3-methylphenyl)piperidin-4-one (MBMP) molecule

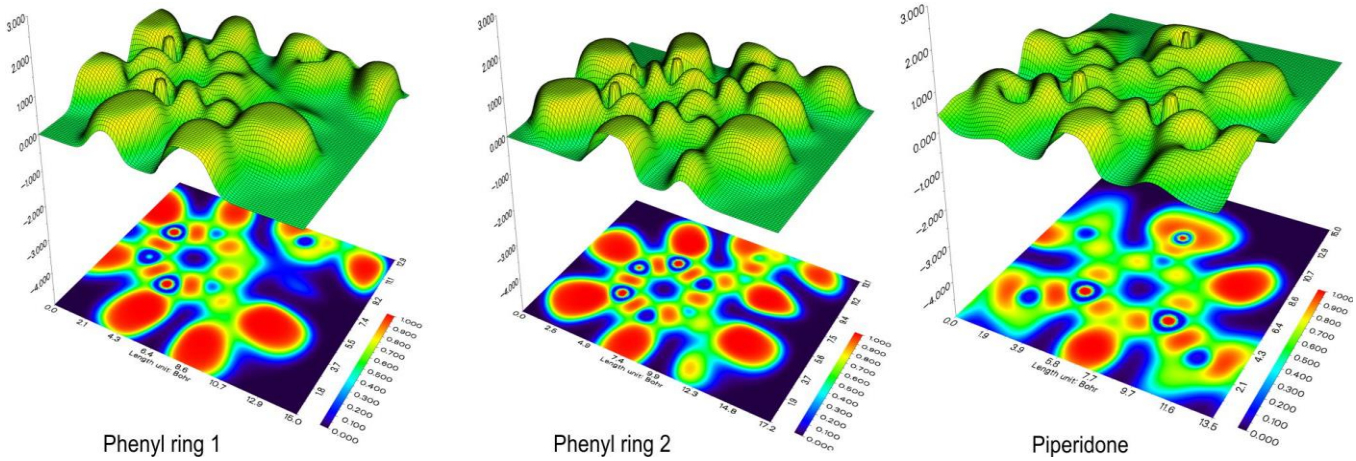

Fig. 9. Shaded surface map of 3-methyl-2,6-*bis*(3-methylphenyl)piperidin-4-one (MBMP) molecule

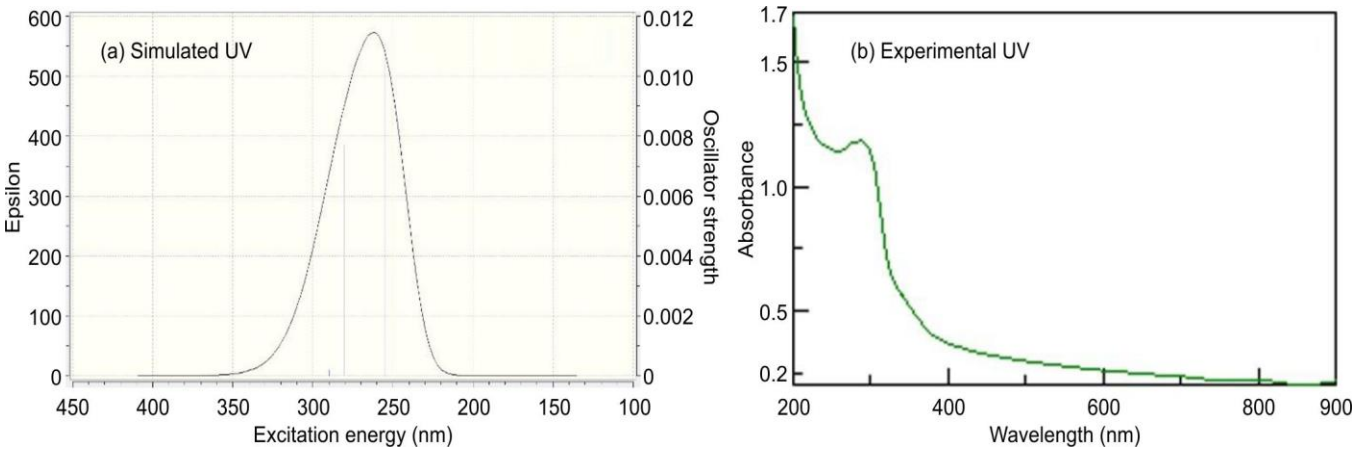

Fig. 10. UV-Vis spectra (a) simulated and (b) observed for MBMP in ethanol solvent

TABLE-11
SIMULATED UV-VIS DATA OF MBMP MOLECULE IN ETHANOL SOLVENT

Energy (cm^{-1})	Wavelength (nm)		Osc. strength (f)	Major contributions	Minor contributions
	Observed	Calculated			
34506.0	285	289.8	0.0002	HOMO-4 → LUMO (26%), HOMO-3 → LUMO (45%), HOMO-1 → LUMO (11%)	HOMO-4 → LUMO+2 (3%), HOMO-3 → LUMO+2 (5%), HOMO-2 → LUMO (5%)
35618.3	281	280.8	0.0077	HOMO → LUMO (97%)	–
39227.5	247	254.9	0.0111	HOMO-2 → LUMO (19%), HOMO-1 → LUMO (66%)	HOMO-2 → LUMO+1 (2%), HOMO-1 → LUMO+1 (2%)

for ethanol solvent. The TD-DFT method was opted to compute the theoretical UV-Vis spectra in ethanol solvent. The calculated data are summarized in Table-11, with the HOMO of the molecule located at molecular orbital (MO) 79.

The UV-Vis spectrum of the title molecule in ethanol shows three prominent absorption peaks. The simulated wavelengths are observed at 289.8, 280.8 and 254.9 nm, which are in good agreement with the experimental values of 285, 281 and 247 nm, respectively. The peak at 289.8 nm with an energy of 34506.0 cm^{-1} arises due to the major contribution of HOMO-4→LUMO (26%), HOMO-3→LUMO (45%), HOMO-1 →LUMO (11%) and the minor contribution of HOMO-4→ LUMO+2 (3%), HOMO-3→LUMO+2 (5%), HOMO-2→ LUMO (5%). The contribution of HOMO→LUMO (97%) is the only reason for the peak at 280.8 nm with an energy of 35618.3 cm^{-1}. Due to the minor contribution of HOMO-2→ LUMO+1 (2%), HOMO-1→LUMO+1 (2%) and the major contribution of HOMO-2→LUMO (19%), HOMO-1→ LUMO (66%), a peak with energy of 39227.5 cm^{-1} is appeared at 254.9. The three oscillator strengths observed are 0.0002, 0.0077 and 0.0111.

NMR spectral analysis: Tables 12 and 13 provide the theoretical and experimental values for the MBMP's ^{1}H and ^{13}C NMR, respectively. Figs. 11 and 12 show the recorded ^{1}H NMR and ^{13}C NMR spectra (both simulated and observed) in DMSO-d_6 solvent. Theoretical chemical shift values were calculated using the same basis set. In general, more shielded protons resonate upfield (lower chemical shift), while less shielded protons appear downfield (higher chemical shift) [77].

TABLE-12
^{1}H NMR (EXPERIMENTAL AND CALCULATED) CHEMICAL SHIFTS (ppm) OF MBMP MOLECULE

Atom	Experimental (ppm)	B3LYP/6-311G(d,p) (ppm)
H29	7.3656	7.4229
H31	7.3536	6.8735
H34	7.3394	6.7909
H32	7.3275	6.7870
H36	–	6.7596
H35	7.1727	6.6768
H30	7.1483	6.6405
H33	7.1230	6.5546
H25	3.9912	4.6231
H28	3.9570	4.3306
H27	2.9481	3.1561
H23	2.9047	2.9668
H24	2.7378	2.8862
H39	2.4562	2.4704
H42	2.4189	2.3252
H37	2.4106	2.2185
H41	2.3761	2.0400
H38	2.3676	1.9187
H40	2.3401	1.8530
H26	3.3666	1.6684
H45	2.2270	1.1285
H43	2.0843	1.1253
H44	2.0650	0.1888

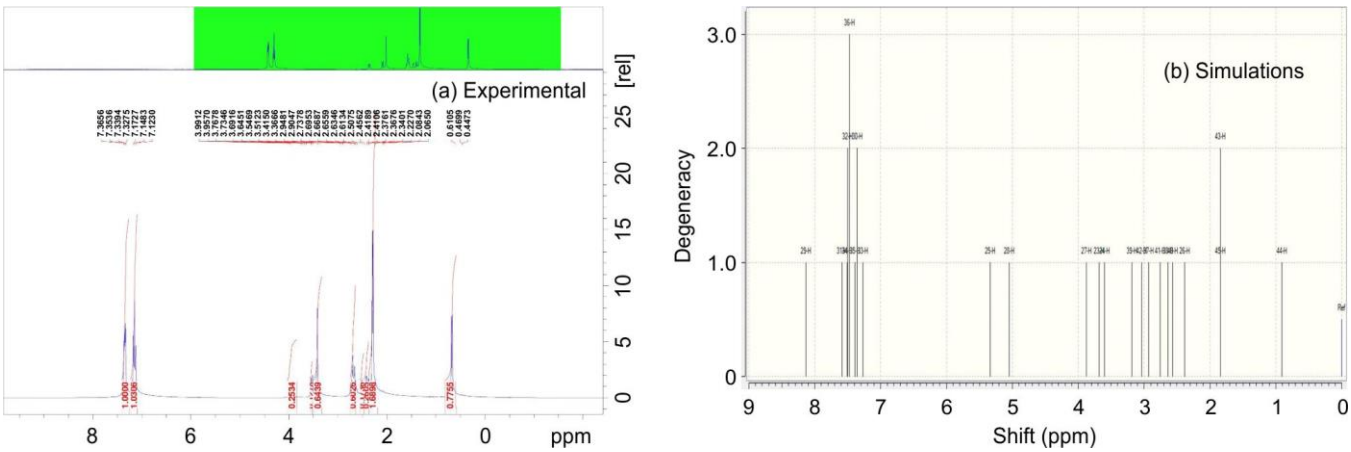

Fig. 11. ^{1}H NMR spectra (experimental and simulated) of MBMP molecule

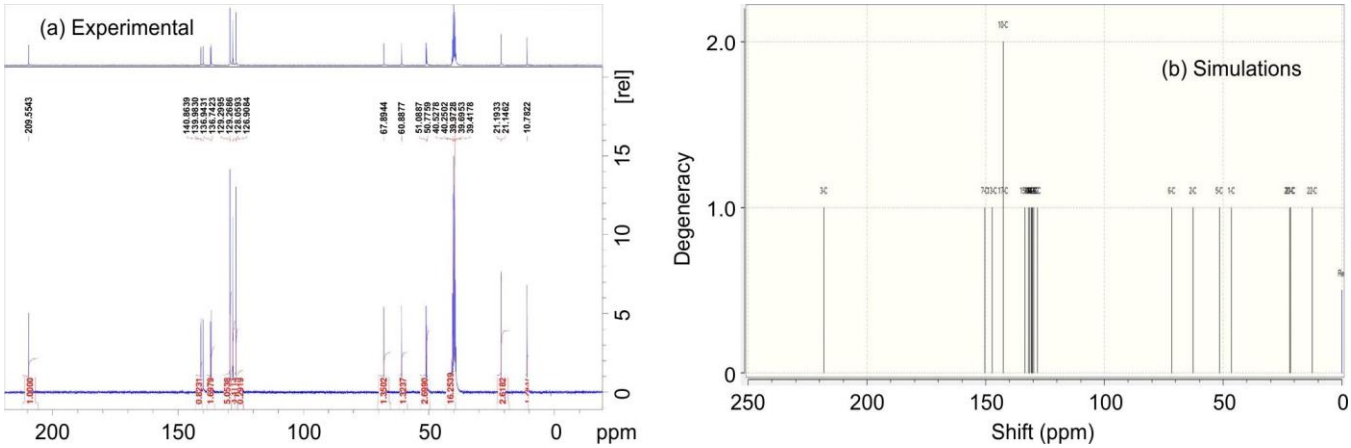

Fig. 12. Experimental and simulated ^{13}C NMR spectra of MBMP molecule

TABLE-13
^{13}C NMR (EXPERIMENTAL AND CALCULATED) CHEMICAL SHIFTS (ppm) OF MBMP MOLECULE

Atom	Experimental (ppm)	B3LYP/6-311G(d,p) (ppm)
C3	209.5543	218.044
C7	140.8639	150.394
C13	139.9830	147.215
C17	136.9431	142.582
C10	136.7423	142.534
C15	129.2995	133.473
C8	–	131.819
C11	129.2686	131.527
C14	–	130.809
C18	128.0593	130.471
C16	–	130.308
C12	126.9084	129.855
C9	–	128.163
C6	67.8944	71.594
C2	60.8877	62.7153
C5	50.7759	51.5471
C1	39.9728	46.4018
C20	21.1933	21.9077
C21	21.1462	21.5833
C22	10.7822	12.4127

^{13}C NMR spectra analysis: The nearby electronegative oxygen atom O19 causes the carbon C3 in the piperidone ring to appear at a greater chemical shift of δ 209.5543 ppm. The piperidone ring has a -CH_2 moiety (C1), which is detected at δ 39.9728 ppm. Aromatic carbon signals are recognised between δ 126.9084 and 140.8639 parts per million. The piperidone ring has a methyl group (C22), which is detected at 10.7822 ppm and appears to be well protected by methyl hydrogens. Two more methyl groups are linked with phenyl rings (C20 and C21) and appear at δ 21.1933 and 21.1462 ppm, respectively. The two carbon atoms, C10 and C17, of two phenyl rings bear two methyl groups (C20 and C21) and they are shown at δ 136.7423 and 136.9431 ppm, respectively. The two carbon atoms (C7 and C13) of phenyl rings attached to the piperidone ring show their signals at δ 140.8639 and 139.9830 ppm. The measured and anticipated chemical shift values are nearly in perfect agreement.

Docking studies: In this study, the ligand–5YOK protein complexes are stabilized through interactions such as C–H bonds, alkyl and π–σ interactions, as well as π–alkyl and π–π stacking interactions. The 2D and 3D diagrams of the molecular interaction of 5YOK protein with 3-methyl-2,6-*bis*(3-methylphenyl)piperidin-4-one (MBMP) are shown in Fig. 13. The docking results of the ligand and 5YOK protein presented in Table-14 suggested a carbon hydrogen bond of GLY(49) with the bond distance of 2.75 Å. There are 4 alkyl bonds, such as ALA(28), VAL(32), ILE(47) and ILE(84) which are hydrophobic in nature with a bond distance of 3.61, 4.48, 5.15 and 4.61 Å and also there are 3 pi-alkyl bonds from the 2,6-aromatic ring, which binds with ALA(28) and VAL(32) which also come under the hydrophobic category with a bond distance of 5.07, 5.45 and 5.48 Å. There is only one pi-sigma

TABLE-14
MOLECULAR DOCKING RESULTS OF MBMP MOLECULE WITH 5YOK PROTEIN

Name	Parent	Distance (Å)	Category	Types	From	From chem	To	To chem
A:GLY49:HA2 - :LIG1:O	Ligand non-bond monitor	2.75478	Hydrogen bond	C-H bond	A:GLY49:HA2	H-Donor	:LIG1:O	H-Acceptor
A:ILE47:HD12 - :LIG1	Ligand non-bond monitor	2.50443	Hydrophobic	Pi-Sigma	A:ILE47:HD12	C-H	:LIG1	Pi-Orbitals
:LIG1 - :LIG1	Ligand non-bond monitor	4.09493	Hydrophobic	Pi-Pi Stacked	:LIG1	Pi-orbitals	:LIG1	Pi-Orbitals
A:ALA28 - :LIG1:C	Ligand non-bond monitor	3.61915	Hydrophobic	Alkyl	A:ALA28	Alkyl	:LIG1:C	Alkyl
:LIG1:C - A:VAL32	Ligand non-bond monitor	4.48400	Hydrophobic	Alkyl	:LIG1:C	Alkyl	A:VAL32	Alkyl
:LIG1:C - A:ILE47	Ligand non-bond monitor	5.15017	Hydrophobic	Alkyl	:LIG1:C	Alkyl	A:ILE47	Alkyl
:LIG1:C - A:ILE84	Ligand non-bond monitor	4.61011	Hydrophobic	Alkyl	:LIG1:C	Alkyl	A:ILE84	Alkyl
:LIG1 - A:ALA28	Ligand non-bond monitor	5.06680	Hydrophobic	Pi-Alkyl	:LIG1	Pi-orbitals	A:ALA28	Alkyl
:LIG1 - A:ALA28	Ligand non-bond monitor	5.45055	Hydrophobic	Pi-Alkyl	:LIG1	Pi-orbitals	A:ALA28	Alkyl
:LIG1 - A:VAL32	Ligand non-bond monitor	5.47858	Hydrophobic	Pi-Alkyl	:LIG1	Pi-orbitals	A:VAL32	Alkyl

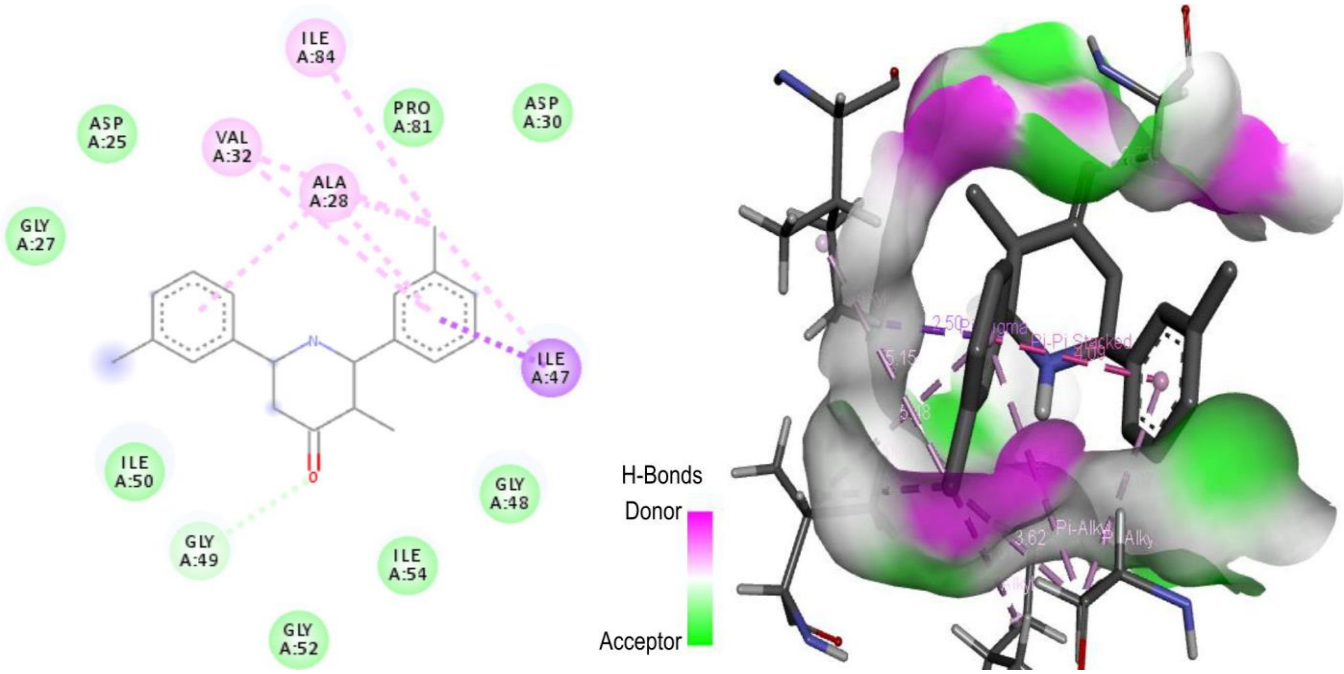

Fig. 13. 2D and 3D docking patterns of 3-methyl-2,6-*bis*(3-methylphenyl)piperidin-4-one (MBMP) molecule

type bond with ILE(47), which is also a hydrophobic category with a bond distance of 2.50 Å.

Conclusion

In this study, 3-methyl-2,6-*bis*(3-methylphenyl)piperidin-4-one (MBMP) was identified as a potential lead compound for anti-retroviral applications. Molecular docking with HIV-1 protease (PDB ID: 5YOK) demonstrated a strong binding affinity, suggesting its possible effectiveness. The molecule was optimized using the B3LYP/6-311G(d,p) level of theory, and its electronic structure was systematically analyzed. Mulliken charge and electrostatic potential (ESP) studies helped identify electron-rich and electron-deficient regions, while HOMO–LUMO analysis provided insight into its stability and reactivity. Fukui function and NBO analyses further revealed reactive sites and stabilization through electron delocalization. NCI and STM studies offered additional understanding of intermolecular interactions and electronic behaviour, while aromaticity analysis confirmed the contribution of phenyl rings. Experimental UV-Vis and NMR results supported the theoretical findings, confirming the structure and purity of the compound. These combined results suggest that MBMP is a promising candidate for further development as an anti-retroviral agent.

ACKNOWLEDGEMENTS

The St. John's College administration generously provided computer and software facilities, for which authors are deeply grateful.

CONFLICT OF INTEREST

The authors declare that there is no conflict of interests regarding the publication of this article.

DECLARATION OF AI-ASSISTED TECHNOLOGIES

During the preparation of this manuscript, the authors used an AI-assisted tool(s) to improve the language. The authors reviewed and edited the content and take full responsibility for the published work.

REFERENCES

1. A. Khajuria, N. Thusu and U. Zutshi, *Phytomedicine*, **9**, 224 (2002); https://doi.org/10.1078/0944-7113-00114
2. A. Wang, C.D. Stout, Q. Zhang and E.F. Johnson, *J. Biol. Chem.*, **290**, 5092 (2015); https://doi.org/10.1074/jbc.M114.627661
3. J. Wójcikowski, P. Maurel and W.A. Daniel, *Drug Metab. Dispos.*, **34**, 471 (2006); https://doi.org/10.1124/dmd.105.006445
4. R.K. Bhardwaj, H. Glaeser, L. Becquemont, U. Klotz, S.K. Gupta and M.F. Fromm, *J. Pharmacol. Exp. Ther.*, **302**, 645 (2002); https://doi.org/10.1124/jpet.102.034728
5. Y.-M. Wang, W. Lin, S.C. Chai, J. Wu, S.S. Ong, E.G. Schuetz and T. Chen, *Toxicol. Appl. Pharmacol.*, **272**, 96 (2013); https://doi.org/10.1016/j.taap.2013.05.014
6. A. Duangjai, K. Tadpetch, V. Rukachaisirikul, C.S. Vaddhanaphuti, and M. Utsintong, *Sci. Pharm.*, **93**, 43 (2025); https://doi.org/10.3390/scipharm93030043
7. S. Wang, H. Li, Z. Lian and S. Deng, *Int. J. Mol. Sci.*, **23**, 7571 (2022); https://doi.org/10.3390/ijms23147571
8. N. Bbosa, P. Kaleebu and D. Ssemwanga, *Curr. Opin. HIV AIDS*, **14**, 153 (2019); https://doi.org/10.1097/COH.0000000000000534
9. V. Guiraud, J. Bocobza, M. Desmonet, F. Damond, J.C. Plantier, G. Moreau, M. Wirden, K. Stefic, F. Barin and A. Gautheret-Dejean, *J. Clin. Microbiol.*, **23**, e00619-23 (2023); https://doi.org/10.1128/jcm.00619-23.
10. W.A. Haseltine, *FASEB J.*, **5**, 2349 (1991); https://doi.org/10.1096/fasebj.5.10.1829694
11. S. Chen, X. Yu and D. Guo, *Viruses*, **10**, 40 (2018); https://doi.org/10.3390/v10010040

12. B.M. Nastri, P. Pagliano, C. Zannella, V. Folliero, A. Masullo, L. Rinaldi, M. Galdiero and G. Franci, *Microorganisms*, **11**, 221 (2023); https://doi.org/10.3390/microorganisms11010221
13. L. Menéndez-Arias and M. Álvarez, *Antiviral Res.*, **102**, 70 (2014); https://doi.org/10.1016/j.antiviral.2013.12.001
14. M. Pereira and N. Vale, *Biomolecules*, **12**, 944 (2022); https://doi.org/10.3390/biom12070944
15. C. Arvieux and O. Tribut, *Drugs*, **65**, 633 (2005); https://doi.org/10.2165/00003495-200565050-00005
16. R. Wang and Q. Zheng, *Langmuir*, **37**, 14407 (2021); https://doi.org/10.1021/acs.langmuir.1c02348
17. K. Karrouchi, E.B. Yousfi, N.K. Sebbar, Y. Ramli, J. Taoufik, Y. Ouzidan, M. Ansar, Y.N. Mabkhot, H.A. Ghabbour and S. Radi, *Int. J. Mol. Sci.*, **18**, 2215 (2017); https://doi.org/10.3390/ijms18112215
18. Y. Kaddouri, F. Abrigach, E.B. Yousfi, M. El Kodadi and R. Touzani, *Heliyon*, **6**, e03185 (2020); https://doi.org/10.1016/j.heliyon.2020.e03185
19. R. Kasibhatta and M.U.R. Naidu, *Drugs R D.*, **8**, 383 (2007); https://doi.org/10.2165/00126839-200708060-00006
20. M.J. Frisch, G.W. Trucks, H.B. Schlegel, G.E. Scuseria, M.A. Robb, J.R. Cheeseman, G. Scalmani, V. Barone, G.A. Petersson, H. Nakatsuji, X. Li, M. Caricato, A.V. Marenich, J. Bloino, B.G. Janesko, R. Gomperts, B. Mennucci, H.P. Hratchian, A.F. Izmaylov, J.L. Sonnenberg, J.V. Ortiz, D. Williams-Young, F. Ding, F. Lipparini, F. Egidi, J. Goings, B. Peng, A. Petrone, T. Henderson, D. Ranasinghe, V.G. Zakrzewski, J. Gao, N. Rega, G. Zheng, W. Liang, M. Hada, M. Ehara, K. Toyota, R. Fukuda, J. Hasegawa, M. Ishida, T. Nakajima, Y. Honda, O. Kitao, H. Nakai, T. Vreven, K. Throssell, J. A. Montgomery Jr., J.E. Peralta, F. Ogliaro, M.J. Bearpark, J.J. Heyd, E.N. Brothers, K.N. Kudin, V.N. Staroverov, T.A. Keith, R. Kobayashi, J. Normand, K. Raghavachari, A.P. Rendell, J.C. Burant, S.S. Iyengar, J. Tomasi, M. Cossi, J.M. Millam, M. Klene, C. Adamo, J.W. Ochterski, R.L. Martin, K. Morokuma, R. Cammi, O. Farkas, J.B. Foresman and D. J. Fox, Gaussian 16, Revision C.01, Gaussian, Inc., Wallingford CT (2016).
21. R.G. Parr and W. Yang, Density Functional Theory of Atoms and Molecules, Oxford University Press, New York (1989).
22. R. Dennington, T.A. Keith and J.M. Millam, GaussView, Version 6.1, Semichem Inc., Shawnee Mission, KS, 2016.
23. I.K. McDonald and J.M. Thornton, *J. Mol. Biol.*, **238**, 777 (1994); https://doi.org/10.1006/jmbi.1994.1334
24. R.D. Cramer, D.E. Patterson and J.D. Bunce, *J. Am. Chem. Soc.*, **110**, 5959 (1988); https://doi.org/10.1021/ja00226a005
25. T. Lu and F. Chen, *J. Comput. Chem.*, **33**, 580 (2012); https://doi.org/10.1002/jcc.22885
26. W. Humphrey, A. Dalke and K. Schulten, *J. Mol. Graph.*, **14**, 33 (1996); https://doi.org/10.1016/0263-7855(96)00018-5
27. C.R. Noller and V. Baliah, *J. Am. Chem. Soc.*, **70**, 3853 (1948); https://doi.org/10.1021/ja01191a092
28. K. Hidaka, T. Kimura, R. Sankaranarayanan, J. Wang, K.F. McDaniel, D.J. Kempf, M. Kameoka, M. Adachi, R. Kuroki, J.T. Nguyen, Y. Hayashi and Y. Kiso, *J. Med. Chem.*, **61**, 5138 (2018); https://doi.org/10.1021/acs.jmedchem.7b01709
29. ACD/ChemSketch, Version 2020.1.2, (2020). *Advanced Chemistry Development*, Inc., Toronto, ON, Canada. www.acdlabs.com.
30. M.D. Hanwell, D.E. Curtis, D.C. Lonie, T. Vandermeersch, E. Zurek and G.R. Hutchison, *J. Cheminform.*, **4**, 17 (2012); https://doi.org/10.1186/1758-2946-4-17
31. S. Dallakyan and A.J. Olson, *Methods Mol. Biol.*, **1263**, 243 (2015); https://doi.org/10.1007/978-1-4939-2269-7_19
32. O. Trott and A.J. Olson, *J. Comput. Chem.*, **31**, 455 (2010); https://doi.org/10.1002/jcc.21334
33. DeLano, L. Warren, The PyMOL Molecular Graphics System (2002).
34. J.G. Stuart and J.W. Jebaraj, *Indian J. Chem.*, **62**, 10 (2023); https://doi.org/10.56042/ijc.v62i10.6186
35. P. Rajamani, V. Vijayakumar, N. Sundaraganesan, M. Jeeva and M.S. Boobalan, *Results Chem.*, **3**, 100096 (2021); https://doi.org/10.1016/j.rechem.2021.100096
36. A. Manimekalai, T. Maruthavanan and K. Selvaraju, *Spectrochim. Acta A Mol. Biomol. Spectrosc.*, **97**, 942 (2012); https://doi.org/10.1016/j.saa.2012.07.089
37. K. Pandiarajan, A. Manimekalai and G. Rajarajan, *ChemInform*, **32**, 7 (2001); https://doi.org/10.1002/chin.200107025
38. D.B. Reddy, A.S. Reddy and V. Padmavathi, *Indian J. Chem.*, **38B**, 141 (1999).
39. R. Jeyaraman, T. Ravindran, M. Sujatha and M. Venkatraj, *Indian J. Chem.*, **38**, 52 (1999).
40. A. Ramalingam, M. Kuppusamy, S. Sambandam, M. Medimagh, O.E. Oyeneyin, A. Shanmugasundaram, N. Issaoui and N.D. Ojo, *Heliyon*, **8**, e10831 (2022); https://doi.org/10.1016/j.heliyon.2022.e10831
41. İ. Sıdır, Y.G. Sıdır, M. Kumalar and E. Taşal, *J. Mol. Struct.*, **964**, 134 (2010); https://doi.org/10.1016/j.molstruc.2009.11.023
42. V. Sangeetha, M. Govindarajan, N. Kanagathara, M.K. Marchewka, M. Drozd and G. Anbalagan, *J. Mol. Struct.*, **1054-1055**, 307 (2013); https://doi.org/10.1016/j.molstruc.2013.10.005
43. M. Arockia doss, S. Savithiri, G. Rajarajan, V. Thanikachalam and C. Anbuselvan, *Spectrochim. Acta A Mol. Biomol. Spectrosc.*, **151**, 773 (2015); https://doi.org/10.1016/j.saa.2015.07.024
44. A.E. Reed and F. Weinhold, *J. Chem. Phys.*, **83**, 1736 (1985); https://doi.org/10.1063/1.449360
45. P. Politzer and J.S. Murray, *J. Mol. Struct.*, **376**, 419 (1996); https://doi.org/10.1016/0022-2860(95)09066-5
46. M.D. Esrafili, *Comput. Theor. Chem.*, **1015**, 1 (2013); https://doi.org/10.1016/j.comptc.2013.04.003
47. M.D. Esrafili and F. Mohammadian-Sabet, *Chem. Phys. Lett.*, **628**, 71 (2015); https://doi.org/10.1016/j.cplett.2015.04.013
48. H. Gökce, O. Akyildirim, S. Bahçeli, H. Yüksek and Ö.G. Kol, *J. Mol. Struct.*, **1056–1057**, 273 (2014); https://doi.org/10.1016/j.molstruc.2013.10.044
49. J.S. Murray and K. Sen, Molecular Electrostatic Potentials, Concepts and Applications, Elsevier, Amsterdam, pp. 7-624 (1996).
50. E. Scrocco and J. Tomasi, *Adv. Quantum Chem.*, **11**, 115 (1978); https://doi.org/10.1016/S0065-3276(08)60236-1
51. Z. Zhou and R.G. Parr, *J. Am. Chem. Soc.*, **112**, 5720 (1990); https://doi.org/10.1021/ja00171a007
52. R.G. Pearson, *J. Org. Chem.*, **54**, 1423 (1989); https://doi.org/10.1021/jo00267a034
53. Y. Atalay, D. Avcı and A. Başoğlu, *Struct. Chem.*, **19**, 239 (2008); https://doi.org/10.1007/s11224-007-9278-3
54. C. Elakiya, R. Shankar, S. Vijayakumar and P. Kolandaivel, *Mol. Phys.*, **115**, 895 (2017); https://doi.org/10.1080/00268976.2017.1292012
55. D. Thangamani, R. Shankar, S. Vijayakumar and P. Kolandaivel, *Mol. Phys.*, **114**, 3055 (2016); https://doi.org/10.1080/00268976.2016.1214293
56. S. Uzun, Z. Esen, E. Koç, N.C. Usta and M. Ceylan, *J. Mol. Struct.*, **1178**, 450 (2019); https://doi.org/10.1016/j.molstruc.2018.10.001
57. A.O. Zacharias, A. Varghese, K.B. Akshaya, M.S. Savitha and L. George, *J. Mol. Struct.*, **1158**, 1 (2018); https://doi.org/10.1016/j.molstruc.2018.01.002
58. C. Morell, A. Grand and A. Toro-Labbé, *J. Phys. Chem. A*, **109**, 205 (2005); https://doi.org/10.1021/jp046577a
59. E.D. Glendening, A.E. Reed, J.E. Carpenter, F.A. Weinhold, NBO, Version 3.1, 1995.
60. R. Naaman and Z. Vager, *Top. Curr. Chem.*, **298**, 237 (2010); https://doi.org/10.1007/128_2010_91
61. J.N. Liu, Z.R. Chen and S.-F. Yuan, *J. Zhejiang Univ. Sci. B*, **6**, 584 (2005); https://doi.org/10.1631/jzus.2005.B0584
62. L. Li, C. Wu, Z. Wang, L. Zhao, Z. Li, C. Sun and T. Sun, *Spectrochim. Acta A Mol. Biomol. Spectrosc.*, **136**, 338 (2015); https://doi.org/10.1016/j.saa.2014.08.153
63. R.Z. Khaliullin, A.T. Bell and M. Head-Gordon, *Chem. Eur. J.*, **15**, 851 (2009); https://doi.org/10.1002/chem.200802107
64. A. Chakraborty, R. De and N. Guchhait, *Chem. Phys. Lett.*, **432**, 616 (2006); https://doi.org/10.1016/j.cplett.2006.10.107

65. B.K. Paul, N. Ghosh, R. Mondal and S. Mukherjee, *Photochem. Photobiol. Sci.*, **14**, 1147 (2015); https://doi.org/10.1039/c5pp00033e
66. B.K. Paul and N. Guchhait, *Comput. Theor. Chem.*, **972**, 1 (2011); https://doi.org/10.1016/j.comptc.2011.06.004
67. E.R. Johnson, S. Keinan, P. Mori-Sánchez, J. Contreras-García, A.J. Cohen and W. Yang, *J. Am. Chem. Soc.*, **132**, 6498 (2010); https://doi.org/10.1021/ja100936w
68. J. Chakraborty, *Heliyon*, **8**, e11408 (2022); https://doi.org/10.1016/j.heliyon.2022.e11408
69. J. Contreras-García, W. Yang and E.R. Johnson, *J. Phys. Chem. A*, **115**, 12983 (2011); https://doi.org/10.1021/jp204278k
70. J. Poater, M. Duran, M. Solà and B. Silvi, *Chem. Rev.*, **105**, 3911 (2005); https://doi.org/10.1021/cr030085x
71. C.W. Bird, *Tetrahedron*, **41**, 1409 (1985); https://doi.org/10.1016/S0040-4020(01)96543-3
72. E. Matito, M. Duran and M. Solà, *J. Chem. Phys.*, **122**, 014109 (2005); https://doi.org/10.1063/1.1824895
73. T.M. Krygowski, *J. Chem. Inf. Comput. Sci.*, **33**, 70 (1993); https://doi.org/10.1021/ci00011a011
74. N. Sablon, F. De Proft, M. Solà and P. Geerlings, *Phys. Chem. Chem. Phys.*, **14**, 3960 (2012); https://doi.org/10.1039/c2cp23372j
75. B. Donner, M. Kleber, C. Bracher and H.J. Kreuzer, *Am. J. Phys.*, **73**, 690 (2005); https://doi.org/10.1119/1.1930867
76. H.L. Schmider and A.D. Becke, *J. Mol. Struct. THEOCHEM*, **527**, 51 (2000); https://doi.org/10.1016/S0166-1280(00)00477-2
77. G. Velraj, S. Soundharam and C. Sridevi, *J. Mol. Struct.*, **1060**, 156 (2014); https://doi.org/10.1016/j.molstruc.2013.12.040